Electronic Supplementary Information for

Square-Planar Imido Complexes of Co: Synthesis, Reactivity and Computational Study

Jackson A. Reyna,[a] V. Mahesh Krishnan,[a,b] Roberto Silva Villatoro,[a] Hadi D. Arman,[a] Sebastian A. Stoian[c,*] and Zachary J. Tonzetich[a,*]

[a]Department of Chemistry, University of Texas at San Antonio (UTSA), San Antonio, TX 78249
[b]Present address: Eastman Chemical Company, 200 S. Wilcox Dr., Kingsport TN 37660.
[c]Department of Chemistry, University of Idaho, Moscow ID 83844.

*sstoian@uidaho.edu *zachary.tonzetich@utsa.edu

Contents

S1. NMR Spectroscopy

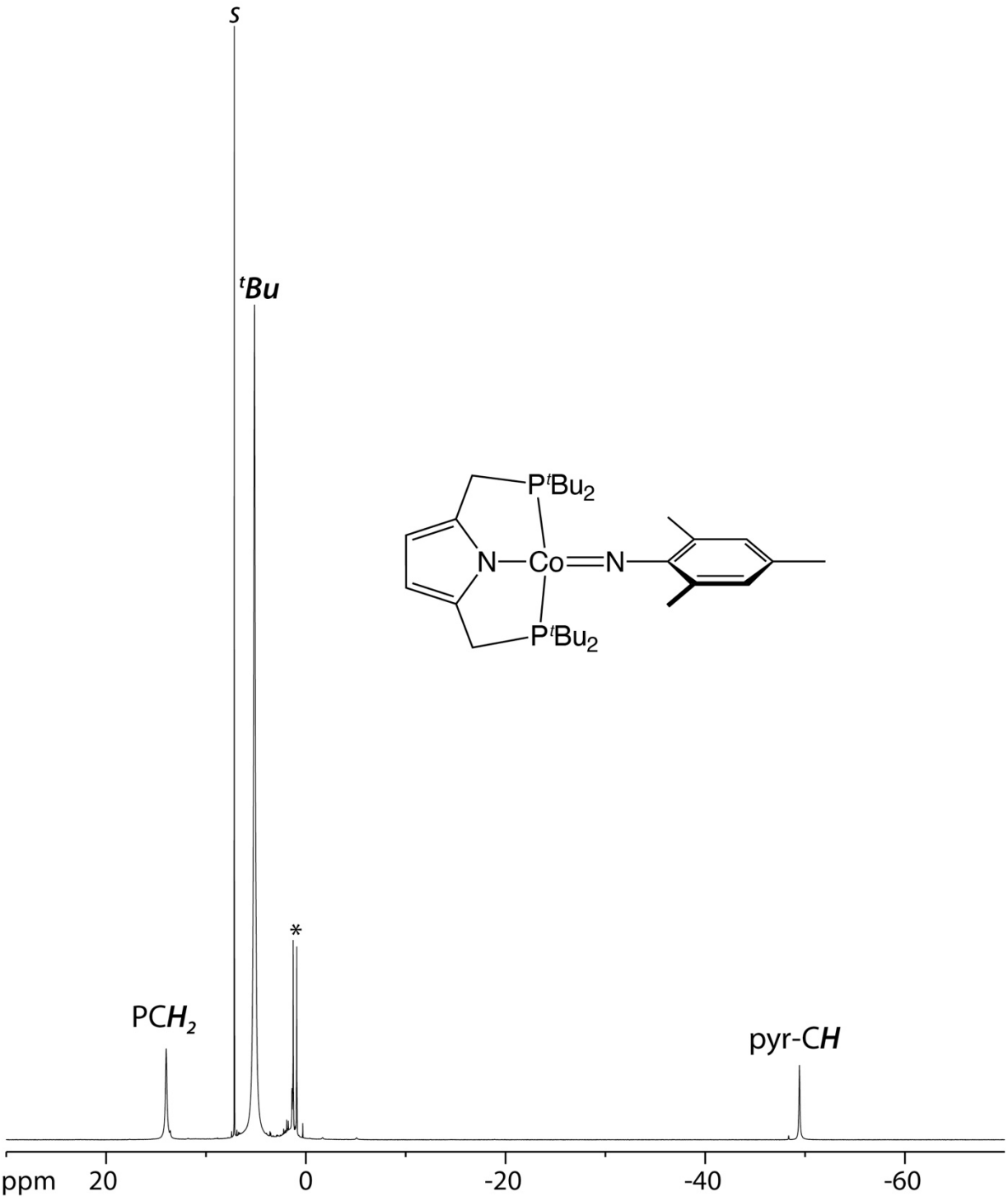

Figure S1. ^{1}H NMR spectrum of **2a**, [Co(NMes)($^{t\text{Bu}}$PNP)], in benzene-d_6 (s). Asterisk denotes small quantity of pentane used in crystallization.

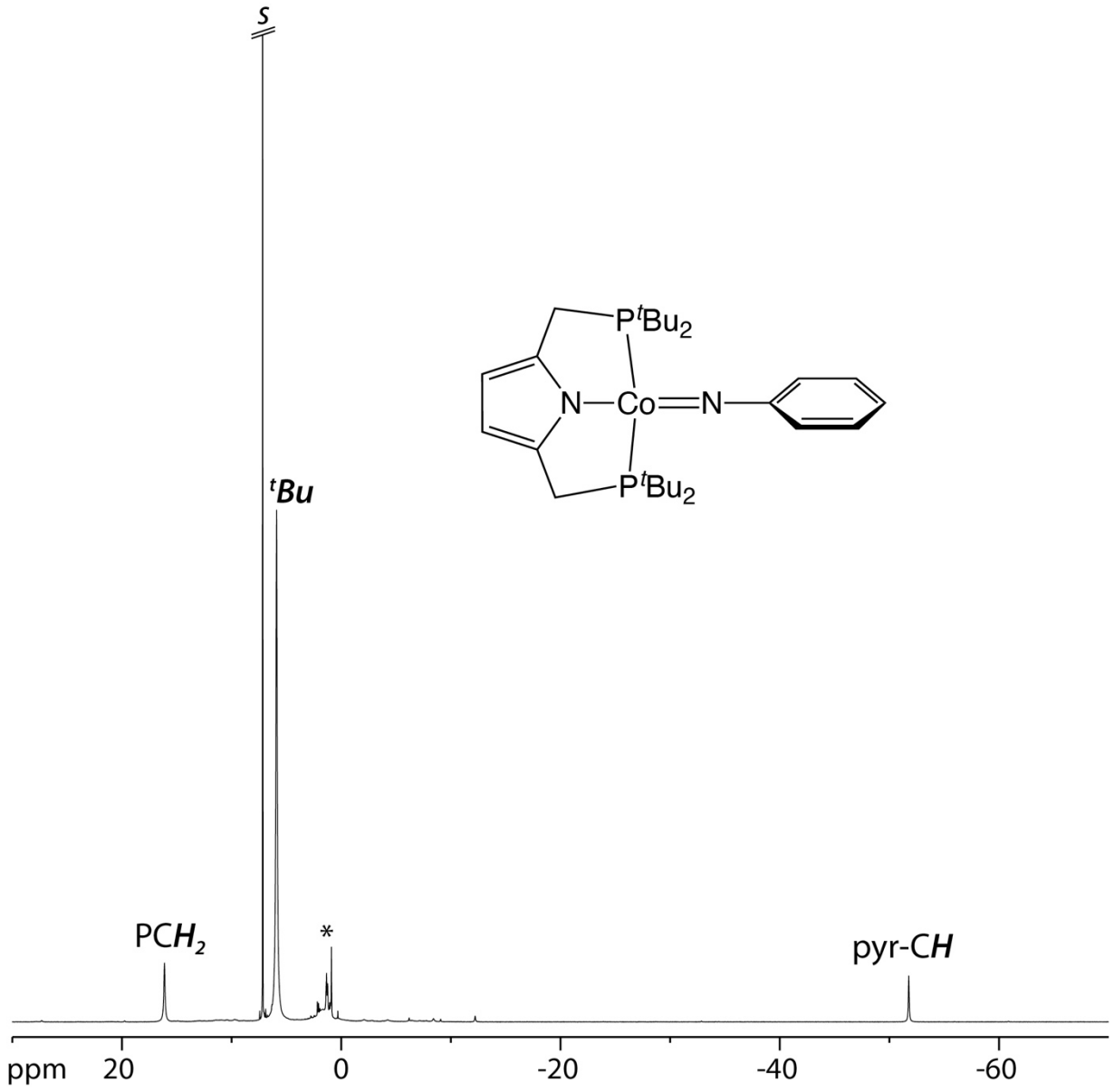

Figure S2. ^{1}H NMR spectrum of **2b**, [Co(NPh)($^{t\text{Bu}}$PNP)], in benzene-d_6 (*s*). Asterisk denotes small quantity of pentane used in crystallization.

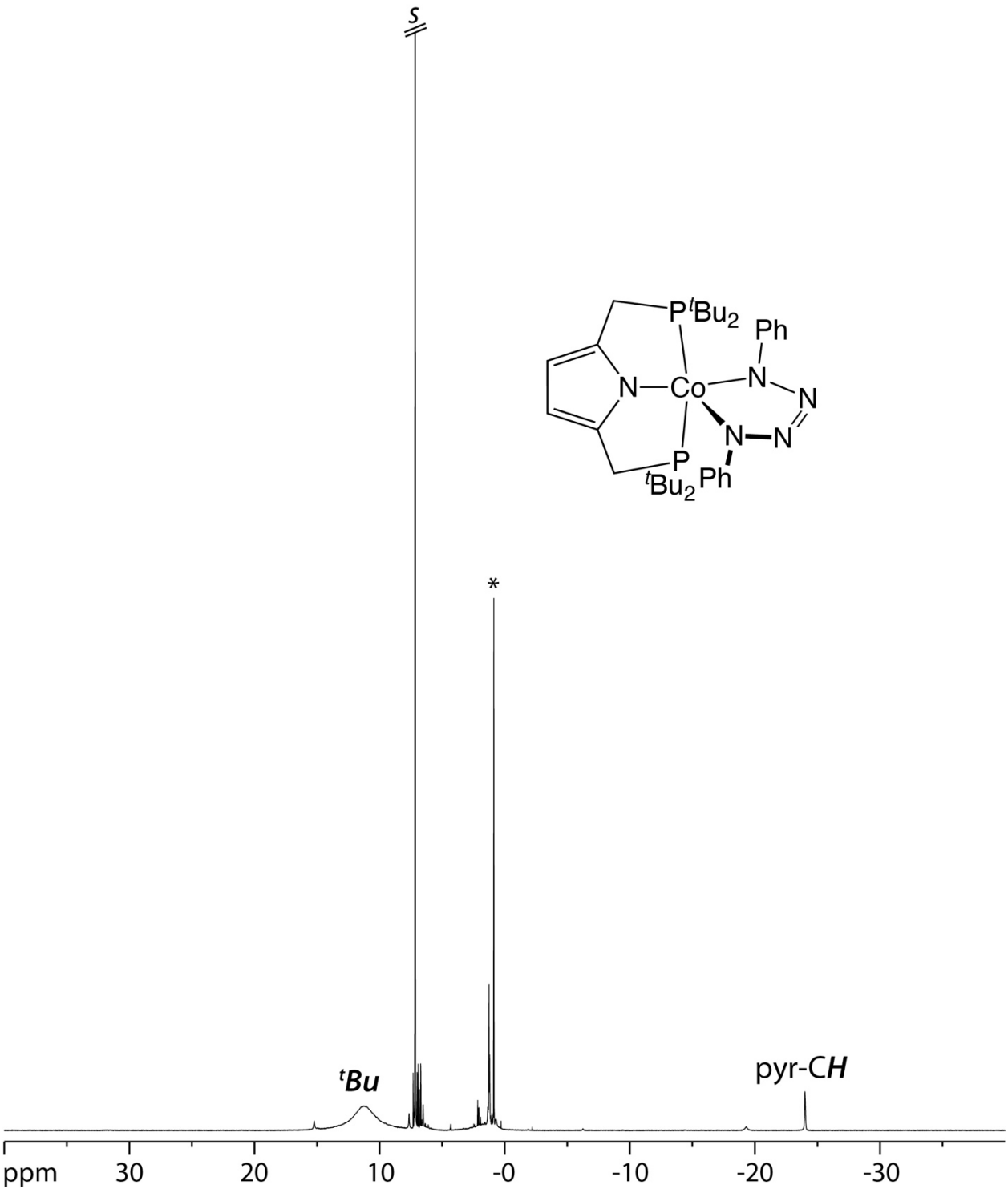

Figure S3. ^{1}H NMR spectrum of **3**, [Co(N_4Ph_2)($^{t\text{Bu}}$PNP)], in benzene-d_6 (*s*). Asterisk denotes small quantity of pentane used in crystallization.

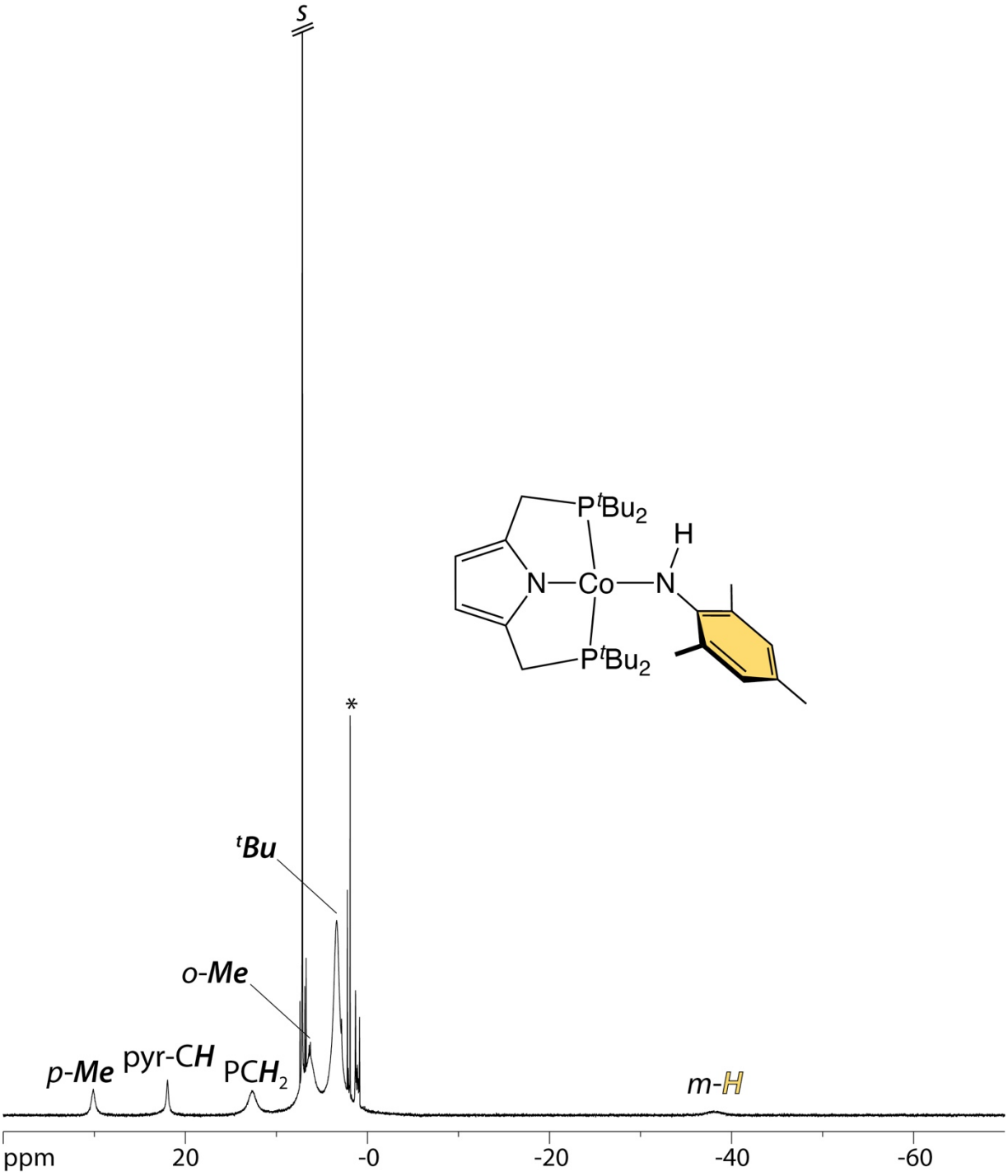

Figure S4. ^{1}H NMR spectrum of **4a**, [Co(NHMes)($^{t\text{Bu}}$PNP)], in benzene-d_6 (*s*). Asterisk denotes small quantity of pentane used in crystallization.

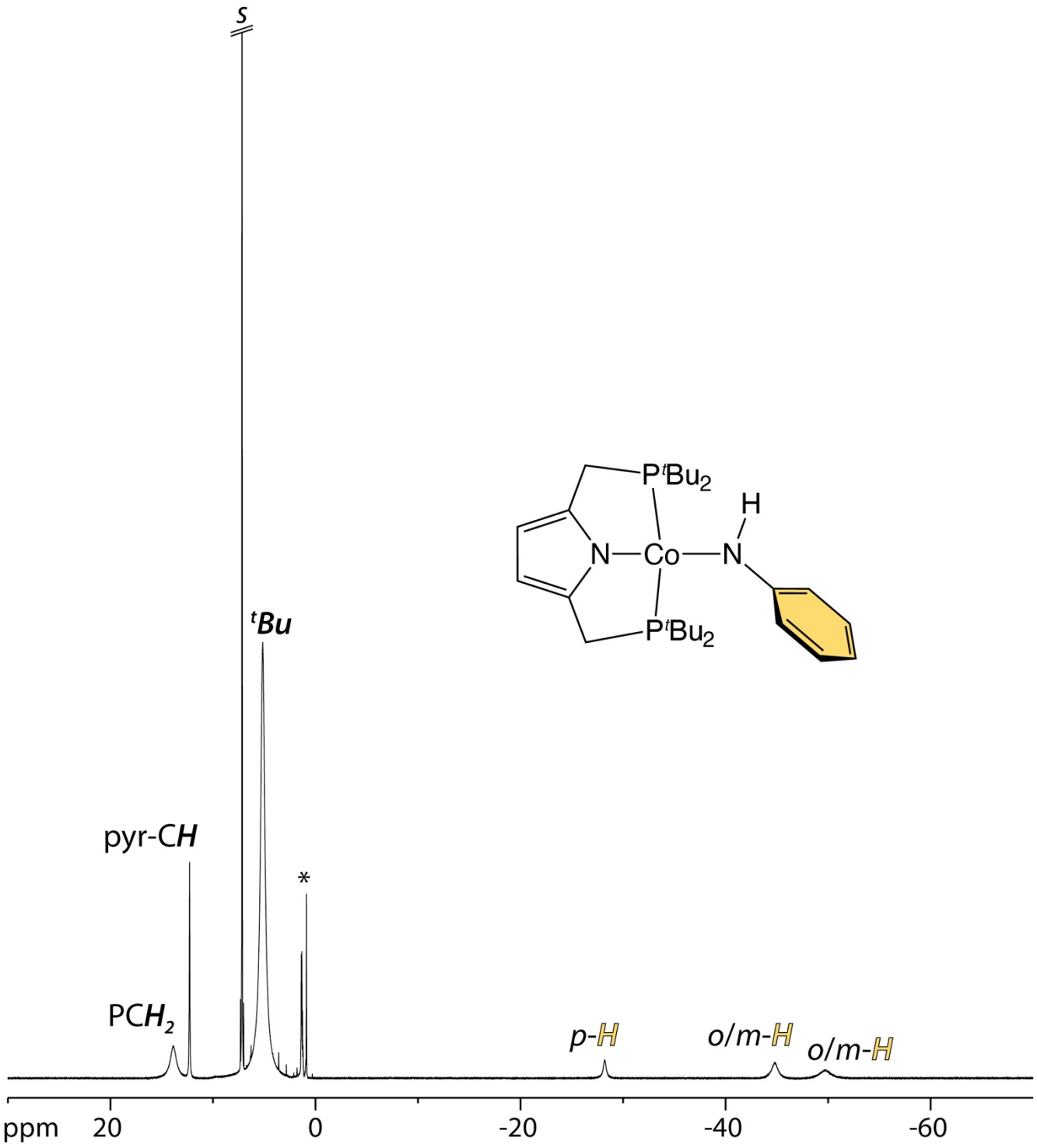

Figure S5. ^{1}H NMR spectrum of **4b**, [Co(NHPh)($^{t\text{Bu}}$PNP)], in benzene-d_6 (*s*). Asterisk denotes small quantity of pentane used in crystallization.

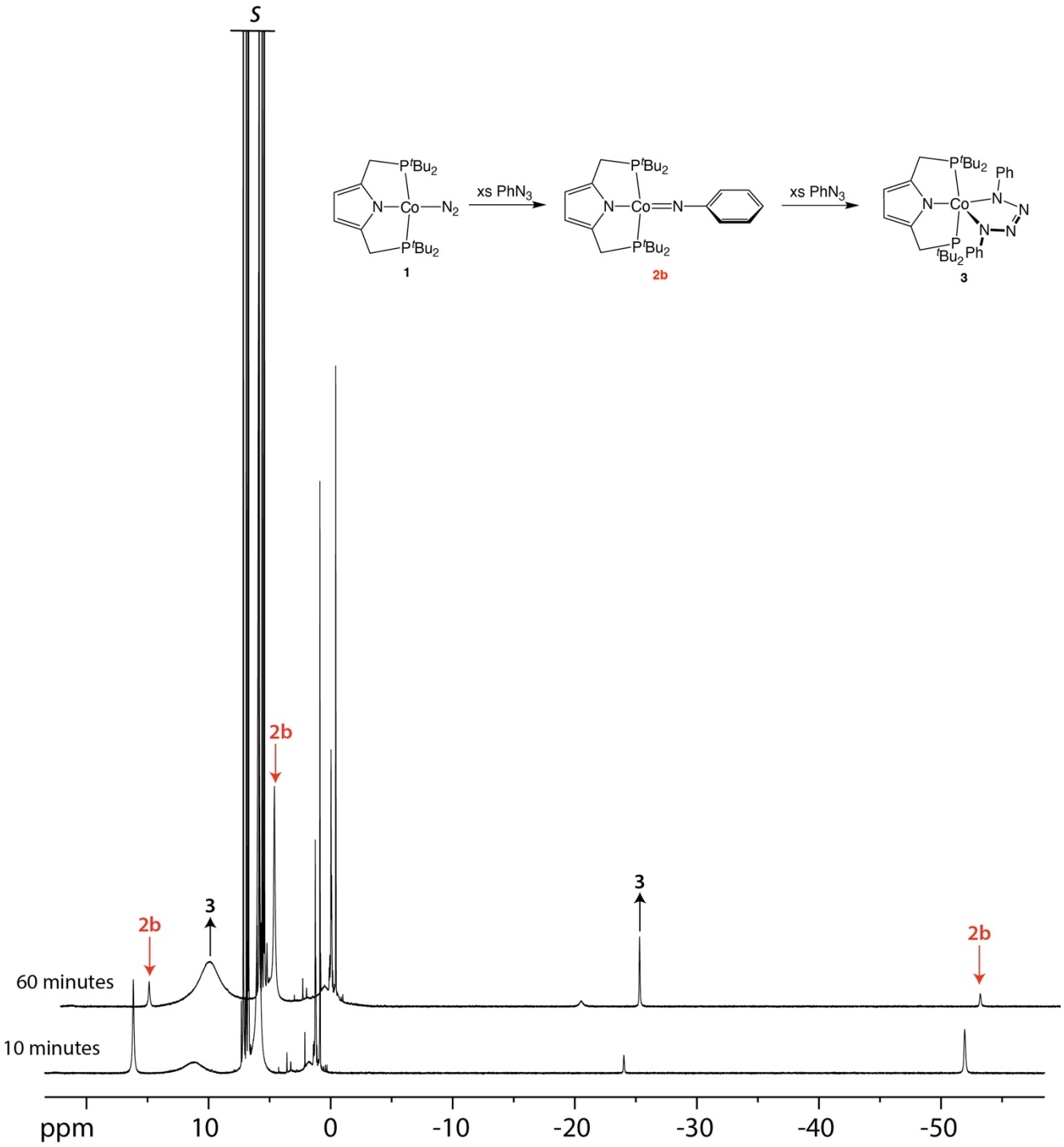

Figure S6. ^{1}H NMR spectrum resulting from the addition of excess PhN_3 to **1** in benzene-d_6 showing successive formation of **2b** followed by **3** after 60 minutes.

S2. Cyclic voltammetry

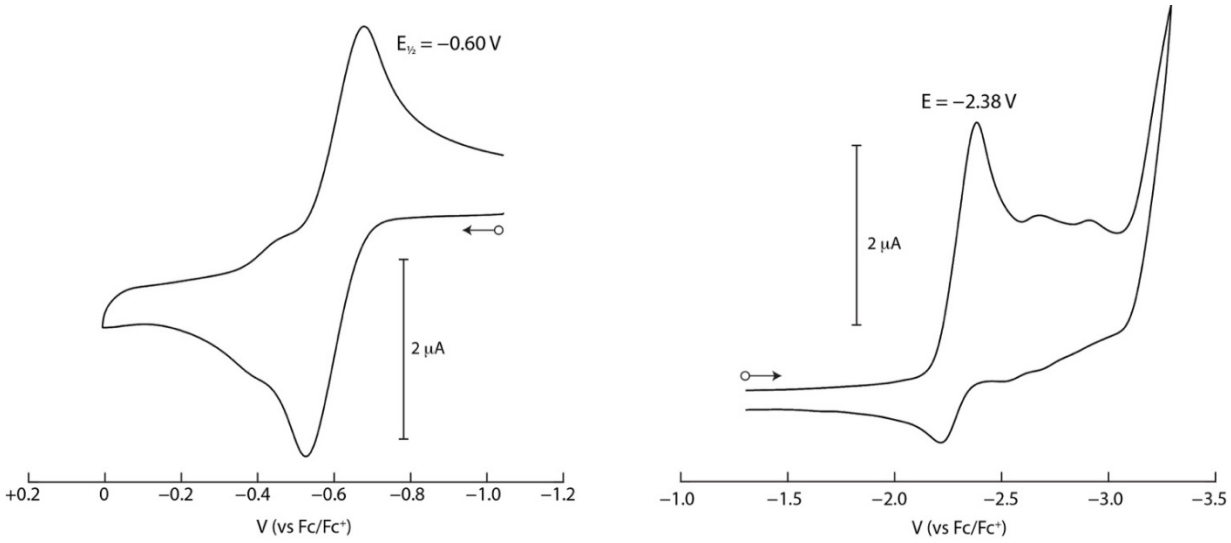

Figure S7. Cyclic voltammogram of **2a** at a Pt disk electrode in THF. Scan rate is 50 mV/s and the supporting electrolyte is 0.2 M Bu_4NPF_6.

S3. X-ray crystallography

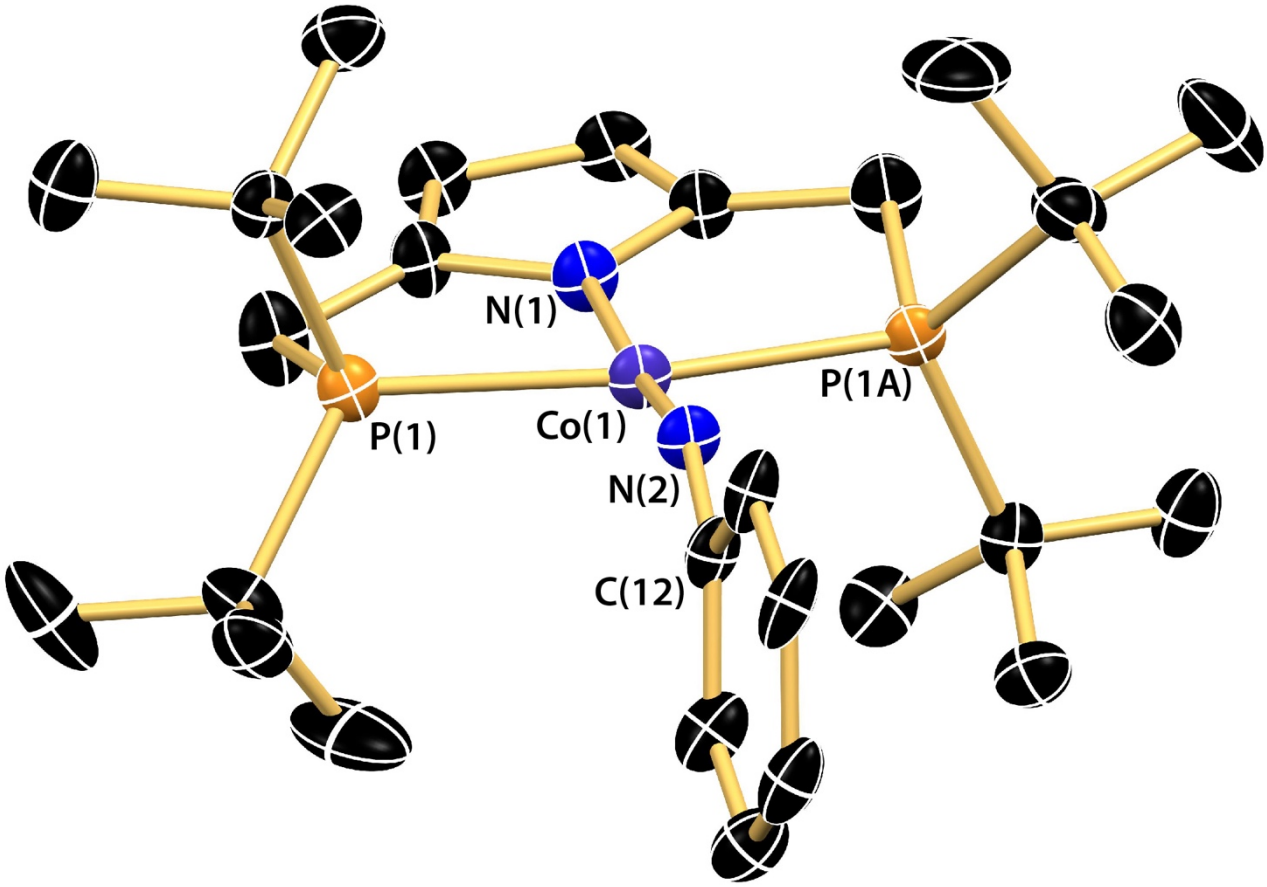

Figure S8. Thermal ellipsoid drawing (50%) of the solid-state structure of **2b**. Hydrogen atoms and minor components of the disorder omitted for clarity. Selected bond distances (Å) and angles (deg): Co(1)-N(2) = 1.724(6); Co(1)-N(1) = 1.890(6); Co-P_{avg} = 2.2454(13); N(2)-C(12) = 1.320(9); N(1)-Co(1)-N(2) = 171.5(3); P(1)-Co(1)-P(2) = 165.97(7); Co(1)-N(2)-C(12) = 155.24(10).

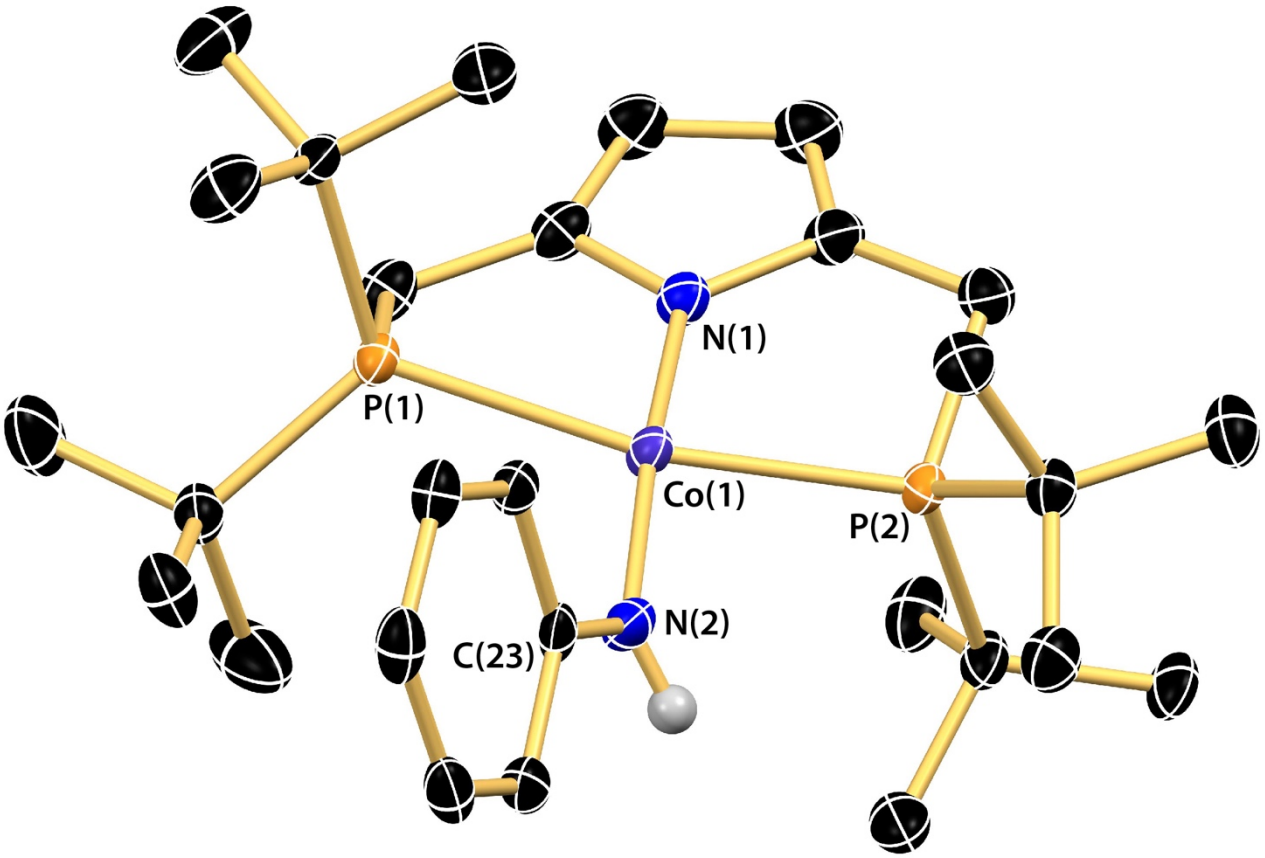

Figure S9. Thermal ellipsoid drawing (50%) of the solid-state structure of **4b**. Hydrogen atom with the exception of that bound to N(2) omitted for clarity. Selected bond distances (Å) and angles (deg): Co(1)-N(2) = 1.880(2); Co(1)-N(1) = 1.875(2); Co(1)-P(1) = 2.3225(8); Co(1)-P(2) = 2.2300(8); N(2)-C(23) = 1.369(4); N(1)-Co(1)-N(2) = 172.96(11); P(1)-Co(1)-P(2) = 164.70(3); Co(1)-N(2)-C(23) = 133.0(2).

Table S1. Crystallographic data and refinement parameters for **2a**, **2b**, **3**, **4a**, and **4b**.[†]

Compound	**2a**	**2b**	**3·C$_6$H$_6$**	**4a**	**4b**
Formula	$C_{31}H_{53}CoN_2P_2$	$C_{28}H_{47}CoN_2P_2$	$C_{40}H_{58}CoN_5P_2$	$C_{31}H_{54}CoN_2P_2$	$C_{28}H_{48}CoN_2P_2$
FW (g/mol)	574.62	532.54	729.78	575.63	533.55
System, space group	monoclinic, $P2_1/c$	monoclinic, $C2/c$	monoclinic, $P2_1/c$	triclinic, $P\bar{1}$	monoclinic, $P2_1/n$
Source	Cu K_α	Cu K_α	Cu K_α	Cu K_α	Mo K_α
Temperature (K)	100.0(1)	100.0(1)	100.0(1)	100.0(1)	98.0(1)
Unit Cell Parameters (Å, deg)	a = 10.46810(10) b = 15.3341(2) c = 19.6726(2) β = 102.577(1)	a = 15.8666(12) b = 13.3021(8) c = 14.6700(13) β = 112.540(10)	a = 19.1588(3) b = 9.92290(10) c = 20.4294(2) β = 93.9130(10)	a = 8.2605(2) b = 12.7200(2) c = 15.1520(3) α = 82.9900(10) β = 87.941(2) γ = 78.642(2)	a = 10.4942(3) b = 13.3791(4) c = 20.8730(6) β = 99.876(3)
Volume (Å^3)	3082.05(6)	2859.7(4)	3874.80(8)	1549.11(6)	2887.20(15)
Z	4	4	4	2	4
Calc. ρ (g/cm^3)	1.238	1.237	1.251	1.234	1.227
F(000)	1240	1144	1560	622	1148
Crystal (mm)	0.12×0.01×0.04	0.12×0.06×0.04	0.13×0.06×0.03	0.16×0.05×0.05	0.37×0.17×0.13
Θ range (deg)	3.689 to 76.558	4.482 to 72.422	2.344 to 74.383	2.939 to 77.957	1.816 to 26.500
Limiting indices	−13 ≤ h ≤ 12 −19 ≤ k ≤ 17 −23 ≤ l ≤ 24	−18 ≤ h ≤ 19 −16 ≤ k ≤ 16 −17 ≤ l ≤ 17	−23 ≤ h ≤ 24 −10 ≤ k ≤ 12 −25 ≤ l ≤ 24	−10 ≤ h ≤ 7 −16 ≤ k ≤ 16 −19 ≤ l ≤ 18	−13 ≤ h ≤ 13 −12 ≤ k ≤ 16 −26 ≤ l ≤ 26
Data / unique	35706 / 6280	12532 / 2698	44268 / 7672	35236 / 6334	20631 / 5983
Completeness	96.8%	99.0%	94.3%	95.5%	99.95%
Data / restraints / parameters	6280 / 0 / 340	2698 / 0 / 182	7672 / 0 / 433	6334 / 0 / 343	5983 / 0 / 313
Goodness-of-fit	1.036	1.087	1.086	1.072	1.137
Final R indices [I > 2σ(I)] R indices (all data)	R_1 = 0.0322, wR_2 = 0.0776 R_1 = 0.0343, wR_2 = 0.0787	R_1 = 0.0859, wR_2 = 0.1546 R_1 = 0.0909, wR_2 = 0.1566	R_1 = 0.0435, wR_2 = 0.0966 R_1 = 0.0498, wR_2 = 0.0992	R_1 = 0.0352, wR_2 = 0.0887 R_1 = 0.0367, wR_2 = 0.0894	R_1 = 0.536 wR_2 = 0.1107 R_1 = 0.0622, wR_2 = 0.1157
Residuals (e·Å^{-3})	0.282 / −0.294	0.772 / −0.540	0.456 / −0.389	0.529 / −0.489	0.557 / −0.361

[†]Refinement method was full-matrix least-squares on F^2. $R_1 = \sum||F_o|-|F_c||/\sum|F_o|$; $wR_2 = (\sum[w(F_o^2-F_c^2)^2]/\sum[w(F_o^2)^2])^{½}$.

S4. Computational studies

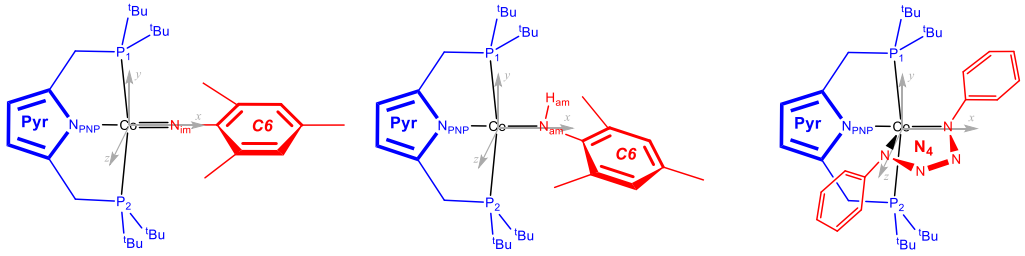

Scheme S1. Labels used for computational results tables. Thus, shown in blue is the $^{t\mathrm{Bu}}$PNP ligand and in red the co-ligand. Pyr indicates the pyrrole core of $^{t\mathrm{Bu}}$PNP, C6 the benzenic core of L_{im}/L_{am} and N_4 the tetraazene moiety of the tetrazido complex.

Computational Details. DFT calculations used the BP86,[1] B3LYP[2] and TPSSH[3] functionals. While the runs involving the hybrid B3LYP and TPSSH functionals relied on the RIJCOSX approximation, the BP86 calculations used the Split-RI-J approximation. The structural models employed in this study were derived from the corresponding experimental X-ray structures. These structures were used both for stand-alone, single point calculations and as starting point for geometry optimizations. The ground state character of a predicted electronic configuration was assessed using time-dependent (TD) DFT calculation such that all predicted one electron excitations were found to have positive energies. For the cases where the SCF led to an excited state, the corresponding negative TD excitation energies were removed by performing a series of orbital swaps, using the *rotate* keyword of the *scf* block, followed by subsequent SCF and TD DFT calculations. The characters of the predicted electronic configurations was inferred by inspecting the results of the Mulliken, Löwdin and natural population analyses.[4] The later analysis was performed using the NBO 7 program.[5] Finally, theoretical zero-field splitting (ZFS) and g tensors were derived from coupled-perturbed (CP) calculations.[6,7]

Ab initio CASSCF calculations were performed using unabridged and simplified structural models derived from the experimental X-ray structures. The initial guesses were derived from restricted open shell, requested using the *roks* keyword, BP86/def2-TZVPP calculations. The active spaces of the initial CAS(*n*,*m*) runs, where *n* are the number of orbitals and *m* the number of electrons, were spanned by the molecular orbitals (MOs) with a contribution from the 3d cobalt orbitals larger than 10 %. These initial runs provided much purer MOs which allowed us to reduce the size of the active spaces of the subsequent calculations. The imido, **2a** complex was investigated using a series of CAS(8,12) calculations for which the active space was spanned by the bonding and antibonding σ orbitals with a $3dx^2\text{-}y^2$ parentage, the non-bonding $3dz^2$ and $3dyz$ orbitals, and the bonding and antibonding sets of two π-orbitals resulted from the interaction of the cobalt based {$3dxy$, $3dxz$} with the {p*z*, p*y*} orbitals localized on the N atom of the imido ligand. In this case we used a simplified structural model obtained by replacing the four ^{t}Bu groups of the PNP ligand with Me, and the methyl groups of the imido co-ligand with H atoms. The CASSCF calculations of the amido complex, **4a** also used a simplified model for which the ^{t}Bu groups were replaced with Me. In this case, the CAS(7,11) active space was spanned by the σ/σ* MOs involving the $3dx^2\text{-}y^2$ cobalt orbital, the remining 3d cobalt orbitals which are essentially non-bonding and a N p-type orbital orthogonal to the CNH plane of the amido coligand. Finally, for the tetrazene complex **3** we used an unabridged structural model and an CAS(7,10) active space spanned five canonical 3d cobalt orbitals including the σ* antibonding MO with a strong $3dx^2\text{-}y^2$ character, the σ-bonding ligand based orbital derived from $3dx^2\text{-}y^2$ and the SOMO orbital of the S = 1/2 monoanionic tetrazene.

For the case of the amido complexes (**4**), the magnetic anisotropy observed by EPR was investigated further using the TD-DFT predicted excited states to obtain theoretical estimates of the $\tilde{\boldsymbol{g}}$ and $\tilde{\boldsymbol{A}}$ tensors using coupled-perturbed (CP) DFT. The TD-DFT suggests that the lowest excited orbital state has an energy of ca. 5000 cm^{-1} and is attained by promoting the spin-down, β electron of the doubly occupied $3d_{z^2}$ orbital to the singly occupied $3d_{xz}$ (Figure S15). Because these two orbital states are mixed by the *y* component of the spin-orbit coupling operator, $\lambda\hat{\boldsymbol{L}}_y\hat{\boldsymbol{S}}_y$, we expect the largest *g*-tensor component to be aligned with the *y* molecular axis. Although this prediction is readily validated by the CP DFT calculations, the corresponding $\Delta g_{max} = g_{max} - g_e$, which ranges from 0.36 obtained using B3LYP to 0.20 predicted by TPSSH, is nearly one order of magnitude smaller than that observed experimentally for **4b**. This difference is likely caused by the fact that TD-DFT overestimates the energies of the lowest excited states. In contrast, our CAS(7,11) calculation suggests that the energy of the first excited state is nearly five times smaller than that predicted by TD-DFT. This lower energy leads to a much larger Δg_{max} value of 1.97, and to a set of theoretical *g* values which are more like the experimental values observed by EPR spectroscopy than those obtained using DFT. Despite the fact that the CAS(7,11) calculations yield charge and spin distributions comparable to those derived from DFT, the order of the two lowest orbital states is switched such that the for the CASSCF ground state the unpaired electron occupies a $3d_{z^2}$ orbital (Figure S16).

Table S2. DFT-predicted relative energies obtained for unabridged structural models derived from the experimental X-ray structures of **2a**, **2b**, **4b** and **3**.

S	Fnct.	Rel. En. [cm^{-1}]	$\langle S^2 \rangle$
Imido, **2a**			
0	b3lyp	1168	1.05
0	rb3lyp	8306	0.00
1	b3lyp	0	2.05
2	b3lyp	9824	6.06
0	bp86	1291	1.01
0	rbp86	5416	0.00
1	bp86	0	2.02
0	tpssh	1169	1.06
0	rtpssh	7428	0.00
1	tpssh	0	2.06
Imido, **2b**			
0	b3lyp	1316	1.04
1	b3lyp	0	2.04
0	bp86	1405	1.01
1	bp86	0	2.02
0	tpssh	1312	1.04
1	tpssh	0	2.05
Amido, **4b**			
1/2	b3lyp	0	0.77
3/2	b3lyp	9619	3.77
1/2	bp86	0	0.76
3/2	bp86	12759	3.76
1/2	tpssh	0	0.78
3/2	tpssh	9986	3.77
Tetrazido, **3**			
0	b3lyp	945	1.02
1	b3lyp	0	2.03
2	b3lyp	7833	6.03
0	bp86	914	0.98
1	bp86	0	2.02
2	bp86	11026	6.02
0	tpssh	803	1.02
1	tpssh	0	2.03
2	tpssh	8748	6.03

Table S3. Ligand and metal charges, see Scheme S2, inferred from the analysis of the Mulliken atomic charges and spins predicted using DFT for the imido complex **2a** and **2b** using an unabridged structural model derived from experimental X-ray structure.

#	Fnct.	Mulliken atomic charges									Mulliken atomic spins					
		b3lyp			bp86			tpssh			b3lyp		bp86		tpssh	
	S	**0**	**0 (*rks*)**	**1**	**0**	**0 (*rks*)**	**1**	**0**	**0 (*rks*)**	**1**	**0**	**1**	**0**	**1**	**0**	**1**
2a	**Co**	0.096	0.072	0.097	-0.075	-0.089	-0.069	0.186	0.164	0.190	0.794	0.982	0.503	0.914	0.727	0.965
	L_{PNP}	0.215	0.257	0.219	0.310	0.331	0.310	0.106	0.145	0.108	-0.085	-0.003	-0.049	0.038	-0.089	-0.004
	L_{im}	-0.311	-0.329	-0.316	-0.235	-0.242	-0.241	-0.292	-0.308	-0.298	-0.709	1.021	-0.455	1.047	-0.638	1.039
	P_1	0.259	0.242	0.258	0.209	0.194	0.208	0.006	-0.009	0.005	-0.044	-0.004	-0.041	0.002	-0.045	-0.004
	P_2	0.284	0.296	0.282	0.235	0.242	0.232	0.049	0.060	0.046	-0.044	-0.005	-0.042	-0.003	-0.047	-0.004
	Pyr	-0.777	-0.755	-0.776	-0.793	-0.775	-0.793	-0.687	-0.660	-0.686	0.025	0.013	0.053	0.039	0.027	0.018
	N_{PNP}	-0.105	-0.091	-0.104	-0.031	-0.021	-0.032	-0.135	-0.120	-0.135	-0.022	-0.032	-0.012	-0.026	-0.030	-0.038
	N_{im}	-0.387	-0.344	-0.381	-0.259	-0.243	-0.254	-0.359	-0.325	-0.353	-0.339	0.686	-0.078	0.707	-0.275	0.720
	C6	-0.238	-0.268	-0.245	-0.356	-0.368	-0.363	-0.125	-0.155	-0.134	-0.372	0.331	-0.384	0.336	-0.369	0.317
2b	**Co**	0.124		0.127	-0.040		-0.032	0.237		0.244	0.791	1.033	0.482	0.968	0.718	1.019
	L_{PNP}	0.203		0.207	0.305		0.302	0.098		0.099	-0.083	0.003	-0.039	0.051	-0.083	0.003
	L_{im}	-0.326		-0.335	-0.264		-0.270	-0.335		-0.343	-0.708	0.964	-0.443	0.981	-0.635	0.978
	P_1	0.285		0.283	0.234		0.232	0.039		0.037	-0.050	0.000	-0.045	0.005	-0.052	0.002
	P_2	0.270		0.268	0.225		0.222	0.039		0.036	-0.043	-0.003	-0.037	0.003	-0.043	-0.002
	Pyr	-0.813		-0.812	-0.896		-0.896	-0.678		-0.677	0.046	0.045	0.063	0.066	0.055	0.055
	N_{PNP}	-0.082		-0.081	-0.015		-0.016	-0.116		-0.116	-0.020	-0.030	-0.008	-0.024	-0.025	-0.035
	N_{im}	-0.375		-0.373	-0.267		-0.266	-0.374		-0.373	-0.379	0.651	-0.117	0.654	-0.313	0.670
	C6	-1.000		-1.007	-1.153		-1.158	-0.568		-0.576	-0.356	0.332	-0.376	0.359	-0.368	0.344

Table S4. Ligand and metal charges, see Scheme S2, inferred from the analysis of the Löwdin atomic charges and spins predicted using DFT for the imido complex **2a** using an unabridged structural model derived from experimental X-ray structure.

	Löwdin atomic charges						Löwdin atomic spins					
Fnct.	**b3lyp**		**bp86**		**tpssh**		**b3lyp**		**bp86**		**tpssh**	
S	**0**	**1**	**0**	**1**	**0**	**1**	**0**	**1**	**0**	**1**	**0**	**1**
Co	-0.708	-0.708	-0.757	-0.753	-0.722	-0.721	0.731	0.970	0.468	0.898	0.655	0.948
L_{PNP}	0.896	0.901	0.918	0.920	0.898	0.903	-0.037	0.026	0.008	0.075	-0.024	0.043
L_{im}	-0.188	-0.193	-0.161	-0.167	-0.176	-0.182	-0.695	1.003	-0.476	1.027	-0.631	1.009
P_1	1.015	1.015	0.996	0.996	1.003	1.003	-0.032	-0.002	-0.028	0.005	-0.032	0.000
P_2	1.017	1.017	0.998	0.998	1.005	1.005	-0.030	-0.003	-0.025	0.004	-0.029	0.000
Pyr	-0.151	-0.150	-0.124	-0.125	-0.135	-0.135	0.043	0.035	0.072	0.061	0.051	0.043
N_{PNP}	0.210	0.210	0.236	0.236	0.216	0.217	0.005	0.000	0.017	0.012	0.008	0.004
N_{im}	0.088	0.090	0.128	0.128	0.100	0.101	-0.294	0.560	-0.105	0.558	-0.242	0.561
C6	-0.214	-0.219	-0.236	-0.240	-0.212	-0.216	-0.354	0.393	-0.328	0.415	-0.345	0.399

Table S5. Ligand and metal charges, see Scheme S2, inferred from the analysis of the natural atomic charges and spins predicted using DFT for the imido complex **2a** using an unabridged structural model derived from experimental X-ray structure.

	Natural atomic charges						Natural atomic spins					
Fnct.	**b3lyp**		**bp86**		**tpssh**		**b3lyp**		**bp86**		**tpssh**	
S	**0**	**1**	**0**	**1**	**0**	**1**	**0**	**1**	**0**	**1**	**0**	**1**
Co	0.489	0.479	0.312	0.316	0.440	0.433	0.713	0.862	0.421	0.768	0.630	0.831
L_{PNP}	0.106	0.112	0.212	0.209	0.134	0.138	-0.035	0.049	0.008	0.095	-0.022	0.068
L_{im}	-0.595	-0.591	-0.524	-0.525	-0.574	-0.571	-0.678	1.089	-0.429	1.136	-0.608	1.100
P_1	1.070	1.072	1.081	1.080	1.056	1.057	-0.035	0.010	-0.032	0.016	-0.034	0.016
P_2	1.073	1.074	1.084	1.082	1.059	1.059	-0.033	0.010	-0.030	0.015	-0.031	0.016
Pyr	-0.936	-0.935	-0.900	-0.904	-0.919	-0.919	0.045	0.037	0.078	0.065	0.053	0.044
N_{PNP}	-0.569	-0.570	-0.506	-0.510	-0.551	-0.553	0.002	-0.003	0.018	0.009	0.004	0.000
N_{im}	-0.657	-0.642	-0.556	-0.549	-0.630	-0.617	-0.319	0.739	-0.068	0.759	-0.252	0.747
C6	-0.303	-0.312	-0.351	-0.357	-0.315	-0.323	-0.339	0.327	-0.343	0.352	-0.338	0.332

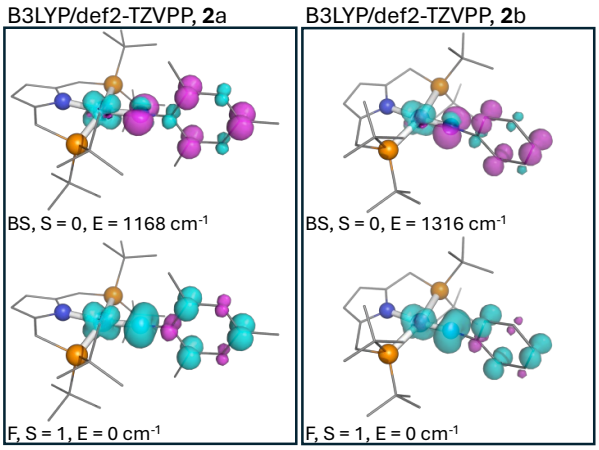

Figure S10. Spin densities plots obtained for **2a** (*left*) and **2b** (*right*) for the F, S = 1 states (*bottom*) and the BS, S = 0 (*top*) at the B3LYP/def2-TZVPP level of theory. Plots were obtained using an isosurface value of ±0.008. α spin density is shown in purple and β spin density is shown in cyan.

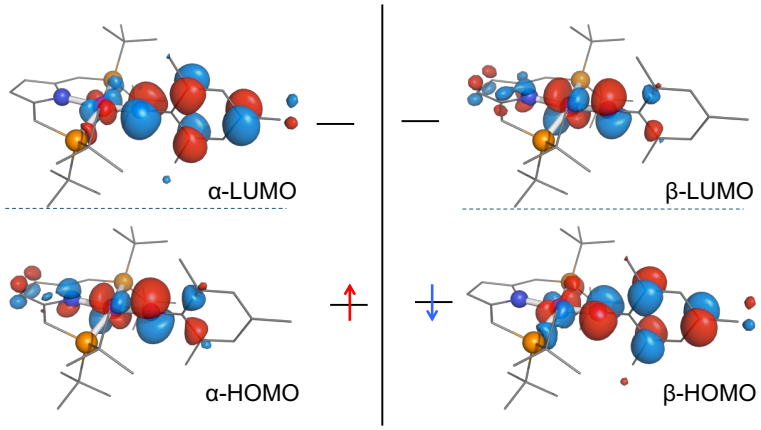

Figure S11. Spin-up, α (*left*) and spin-down, β (*right*) HOMO and LUMO molecular orbitals obtained for the BS, *S* = 0 state of **2a** at the BP86/def2-TZVPP level of theory. The corresponding spin density is shown in the top right corner of Figure S11.

Table S6. DFT-predicted reduced Mulliken orbital charges and spins for the cobalt ion of **2a** using an unabridged structural model derived from the experimental X-ray structure.

	Mulliken reduced orbital charges									Mulliken reduced orbital spins					
Fnct.	**b3lyp**			**bp86**			**tpssh**			**b3lyp**		**bp86**		**tpssh**	
S	**0**	**0 (rks)**	**1**	**0**	**0 (rks)**	**1**	**0**	**0 (rks)**	**1**	**0**	**1**	**0**	**1**	**0**	**1**
dz^2	1.872	1.878	1.878	1.863	1.860	1.866	1.856	1.863	1.861	0.042	0.041	0.025	0.031	0.033	0.033
d*xz*	1.261	1.441	1.290	1.396	1.482	1.411	1.314	1.454	1.339	0.702	0.676	0.548	0.539	0.655	0.633
d*yz*	1.878	1.837	1.876	1.835	1.814	1.834	1.863	1.829	1.863	0.005	0.024	-0.004	0.032	0.004	0.027
dx^2-y^2	0.880	0.899	0.886	1.000	1.009	1.004	0.891	0.904	0.896	0.070	0.059	0.039	0.047	0.071	0.063
d*xy*	1.788	1.664	1.752	1.674	1.619	1.649	1.760	1.668	1.727	-0.079	0.158	-0.154	0.223	-0.104	0.177

Table S7. DFT-predicted reduced Lowdin orbital charges and spins for the cobalt ion of **2a** using an unabridged structural model derived from the experimental X-ray structure.

	Löwdin reduced orbital charges									Löwdin reduced orbital spins					
Fnct.	**b3lyp**			**bp86**			**tpssh**			**b3lyp**		**bp86**		**tpssh**	
S	**0**	**0 (rks)**	**1**	**0**	**0 (rks)**	**1**	**0**	**0 (rks)**	**1**	**0**	**1**	**0**	**1**	**0**	**1**
d*z*²	1.954	1.960	1.960	1.943	1.940	1.946	1.944	1.952	1.950	0.040	0.039	0.024	0.029	0.030	0.031
d*xz*	1.379	1.543	1.405	1.494	1.575	1.508	1.416	1.543	1.438	0.701	0.678	0.554	0.547	0.656	0.637
d*yz*	1.933	1.894	1.932	1.889	1.869	1.888	1.912	1.880	1.912	0.005	0.026	-0.005	0.033	0.003	0.029
d*x*²-*y*²	1.205	1.224	1.211	1.298	1.305	1.303	1.236	1.248	1.241	0.056	0.048	0.032	0.037	0.058	0.048
d*xy*	1.889	1.769	1.855	1.778	1.721	1.755	1.854	1.763	1.824	-0.097	0.177	-0.166	0.235	-0.120	0.196

Table S8. DFT-predicted natural atomic orbital occupancies for the cobalt site and nitrogen atom of the imido ligand of **2a** using an unabridged structural model derived from the experimental X-ray structure.

Fnct.	**S**	**Sp.**	**Co**						**N_{im}**			
			d*xy*	**d*xz***	**d*yz***	**d*x*²-*y*²**	**d*z*²**	**total**	**p*x***	**p*y***	**p*z***	**total**
b3lyp	**0**	α	0.904	0.976	0.979	0.572	0.979	4.409	0.677	0.347	0.905	1.929
		β	0.964	0.316	0.977	0.502	0.944	3.703	0.676	0.818	0.745	2.239
		α+β	1.868	1.292	1.956	1.074	1.923	8.112	1.353	1.165	1.650	4.168
	0 (rks)		1.750	1.492	1.917	1.102	1.932	8.192	1.342	1.249	1.477	4.067
	1	α	0.979	0.977	0.985	0.571	0.980	4.492	0.685	0.830	0.917	2.432
		β	0.853	0.345	0.969	0.513	0.949	3.629	0.665	0.357	0.702	1.725
		α+β	1.832	1.322	1.954	1.084	1.929	8.121	1.350	1.187	1.619	4.156
bp86	**0**	α	0.818	0.968	0.962	0.621	0.973	4.343	0.673	0.432	0.896	2.001
		β	0.953	0.469	0.969	0.584	0.953	3.927	0.658	0.796	0.617	2.072
		α+β	1.771	1.437	1.931	1.205	1.926	8.271	1.331	1.228	1.514	4.073
	0 (rks)		1.724	1.528	1.912	1.214	1.925	8.303	1.329	1.206	1.500	4.036
	1	α	0.968	0.971	0.977	0.626	0.975	4.517	0.678	0.813	0.906	2.397
		β	0.776	0.481	0.953	0.584	0.953	3.748	0.651	0.431	0.589	1.671
		α+β	1.744	1.452	1.930	1.210	1.929	8.265	1.329	1.244	1.495	4.068
tpssh	**0**	α	0.877	0.973	0.973	0.592	0.972	4.387	0.674	0.371	0.901	1.946
		β	0.961	0.364	0.972	0.522	0.946	3.765	0.670	0.815	0.705	2.190
		α+β	1.838	1.338	1.945	1.114	1.917	8.152	1.345	1.185	1.606	4.136
	0 (rks)		1.750	1.493	1.913	1.134	1.929	8.219	1.336	1.239	1.482	4.057
	1	α	0.976	0.974	0.982	0.589	0.974	4.495	0.681	0.827	0.913	2.420
		β	0.829	0.388	0.962	0.533	0.950	3.663	0.662	0.377	0.666	1.705
		α+β	1.805	1.363	1.944	1.123	1.924	8.158	1.342	1.204	1.579	4.126

Table S9. DFT-predicted natural atomic orbital spins for the cobalt site of **2a** using an unabridged structural model derived from the experimental X-ray structure.

Fnct.	**S**	**Co**						**N_{im}**			
		d*xy*	**d*xz***	**d*yz***	**d*x*²-*y*²**	**d*z*²**	**total**	**p*x***	**p*y***	**p*z***	**total**
b3lyp	**0**	-0.061	0.660	0.002	0.070	0.035	0.705	0.001	-0.471	0.160	-0.310
	1	0.126	0.632	0.016	0.058	0.031	0.863	0.019	0.472	0.215	0.707
bp86	**0**	-0.135	0.499	-0.007	0.037	0.020	0.416	0.015	-0.365	0.279	-0.071
	1	0.192	0.490	0.025	0.042	0.022	0.770	0.026	0.383	0.317	0.726
tpssh	**0**	-0.084	0.609	0.000	0.070	0.026	0.621	0.004	-0.444	0.197	-0.244
	1	0.146	0.586	0.020	0.056	0.023	0.832	0.019	0.449	0.247	0.715

Table S10. DFT-predicted Löwdin bond orders for the metal ligand-bonds of **2a**.

Fnct.	S	Co-P_1	Co-P_2	Co-N_{PNP}	Co-N_{im}
b3lyp	0	0.880	0.873	0.829	1.393
	1	0.879	0.872	0.828	1.413
bp86	0	0.911	0.904	0.843	1.460
	1	0.909	0.901	0.840	1.463
tpssh	0	0.896	0.890	0.835	1.423
	1	0.896	0.888	0.833	1.436

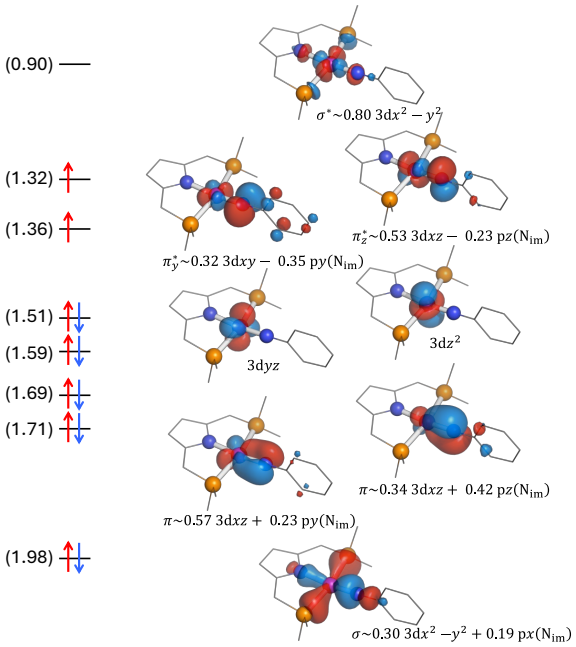

Figure S12. Dominant electronic configuration, that contributes 64.7%, of the ground state predicted by the CAS(8,12) calculations performed for a simplified structural model of **2a**. These calculations considered 25 triplet, S = 1 states and 30 singlet, S = 0 states. The numbers shown in parentheses indicate the predicted Löwdin orbital populations of the corresponding active space orbitals.

Table S11. Spin and charge distributions inferred from the Mulliken population analysis of the CAS(8,12) calculations performed for a simplified structural model of **2a**. The "GS S" entry below indicates the spin of the ground state (root 0).

Nr roots	10 S = 1		25 S = 1 30 S = 0		25 S = 1 10 S = 2		25 S = 1 10 S = 2 30 S = 0	
GS S	1		1		2		2	
Q/S	charge	spin	charge	spin	charge	spin	charge	spin
Co	0.683	1.715	0.675	0.854	0.704	2.300	0.692	1.528
L_{PNP}	-0.210	0.066	-0.675	0.146	-0.704	0.700	-0.692	0.472
L_{im}	-0.474	0.220	0.000	0.000	0.000	0.000	0.000	0.000
P_1	0.247	0.020	0.249	0.010	0.242	0.030	0.245	0.021
P_2	0.206	0.019	0.208	0.010	0.200	0.029	0.204	0.021
Pyr	-0.659	0.020	-0.657	0.010	-0.662	0.029	-0.660	0.020
N_{PNP}	-0.287	0.014	-0.286	0.007	-0.291	0.021	-0.289	0.015
N_{im}	-0.450	0.184	0.000	0.000	0.000	0.000	0.000	0.000
C6	-0.301	0.034	0.000	0.000	0.000	0.000	0.000	0.000

Table S12. Composition of the lowest triplet, *S* = 1 state predicted by the CAS(8,12) calculations of **2a**.

10 S = 1		**25 S = 1 30 S = 0**		**25 S = 1 10 S = 2**		**25 S = 1 10 S = 2 30 S = 0**	
Spin of root 0 = 1		**Spin of root 0 = 1**		**Spin of root 0 = 2**		**Spin of root 0 = 2**	
c	**config**	**c**	**config**	**c**	**config**	**c**	**config**
0.643	22222110	0.647	22222110	0.607	22222110	0.665	22222200
0.052	21122220	0.053	21122220	0.054	21122220	0.162	22022220
0.032	22122120	0.048	22122120	0.048	22222101	0.030	22222110
0.025	22222101	0.035	22222101	0.031	22122120	0.027	22122210
0.019	22222011	0.019	22221111	0.017	22221111	0.027	22221201
0.016	22221111	0.018	21222201	0.017	21122211	0.010	12122211
0.014	22122210	0.018	21122211	0.016	21222201	0.008	12222201
0.013	21122211	0.012	21022221	0.012	22222011	0.008	22021221
0.012	21022221	0.011	11222211	0.012	21022221	0.006	22121211
0.009	21222111	0.009	22022121	0.011	22022121	0.005	22220202
0.009	22111221	0.008	21222210	0.011	11222211	0.005	22221210
0.009	21222201	0.008	22212201	0.011	12222111	0.005	22122120
0.009	11222211	0.008	22111221	0.010	22111221	0.005	22202202
0.008	22220112	0.007	22220112	0.010	22122111	0.003	22212111
0.007	12222111	0.007	22221120	0.009	22212201	0.003	22022211
0.006	22022121	0.007	22211211	0.008	22212210		
0.006	22212210	0.006	12222111	0.008	22220112		
0.005	21122121	0.006	22122111	0.008	21222210		
0.005	21222210	0.005	12122121	0.007	22211211		
0.005	22202112	0.005	22112220	0.006	12122121		
0.004	22122111	0.005	22202112	0.006	22122210		
0.004	22212201	0.004	22212210	0.006	21222120		
0.004	22221120	0.004	22222011	0.006	22221120		
0.004	22211211	0.004	22121121	0.005	22202112		
0.004	22212111	0.004	21212121	0.005	21222111		
0.004	22211121	0.003	22112211	0.003	22112211		
0.004	11222121	0.003	21121221	0.003	22221210		
0.004	22221201	0.003	22211220	0.003	22112220		
0.004	12122121			0.003	21212121		
0.003	21222021			0.003	21121221		
0.003	22022211			0.003	22221201		
0.003	22221210			0.003	22012221		
0.003	22112220			0.003	22211220		
0.003	22112211			0.003	21221211		
0.003	22211220			0.003	20222211		
0.003	21212121						
0.003	21121221						
0.003	22121121						

Table S13. Zero field splitting parameters and g tensors derived from the CAS(8,12) calculations of **2a**. Values obtained using the effective Hamiltonian approach implemented in ORCA.

CAS(8,12)	**GS S**	**D [cm^{-1}]**	**E/D**	**principal g-tensor components**		
10 S = 1	3	41.08	0.321	1.885	2.035	2.429
25 S = 1, 30 S = 0	3	92.04	0.079	1.838	2.024	2.341
25 S = 1, 10 S = 2	5	-41.34	0.022	1.996	2.011	2.562
25 S =1, 10 S =2, 30 S = 0	5	-40.63	0.025	1.996	2.012	2.549

Table S14. Ligand and metal charges, see Scheme S2, inferred from the analysis of the Mulliken atomic charges and spins predicted using DFT for the amido complexes using unabridged structural models derived from experimental X-ray structures.

	Mulliken atomic charges								
Fnct.	**b3lyp**			**bp86**			**tpssh**		
S	**1/2**	**1/2**	**3/2**	**1/2**	**1/2**	**3/2**	**1/2**	**1/2**	**3/2**
Cp.	**4a**	**4b**	**4b**	**4a**	**4b**	**4b**	**4a**	**4b**	**4b**
Co	0.241	0.124	0.207	0.053	-0.055	0.031	0.261	0.202	0.310
L_{PNP}	0.136	0.264	0.116	0.196	0.331	0.169	0.053	0.154	-0.018
L_{am}	-0.994	-0.388	-0.323	-0.959	-0.276	-0.200	-0.688	-0.356	-0.291
P_1	0.244	0.249	0.197	0.190	0.197	0.151	0.012	0.005	-0.050
P_2	0.199	0.201	0.175	0.152	0.155	0.128	-0.014	-0.029	-0.058
N_{PNP}	-0.114	-0.111	-0.130	-0.040	-0.042	-0.067	-0.146	-0.150	-0.179
pyr	-0.794	-0.748	-0.753	-0.813	-0.761	-0.768	-0.697	-0.651	-0.675
N_{am}	-0.364	-0.162	-0.140	-0.271	-0.074	-0.050	-0.374	-0.190	-0.170
H_{am}	0.036	-0.104	-0.102	0.052	-0.077	-0.076	0.072	-0.052	-0.050
C6	-1.034	-1.095	-1.050	-1.163	-1.185	-1.129	-0.602	-0.729	-0.677
Mulliken atomic spins									
Co	0.994	1.025	2.475	0.825	0.868	2.249	0.967	1.009	2.471
L_{PNP}	-0.044	-0.054	0.308	0.006	-0.006	0.406	-0.043	-0.058	0.277
L_{am}	0.040	0.030	0.217	0.142	0.138	0.345	0.062	0.049	0.251
P_1	-0.025	-0.034	0.101	-0.020	-0.028	0.138	-0.025	-0.035	0.104
P_2	-0.022	-0.021	0.078	-0.016	-0.018	0.108	-0.024	-0.022	0.080
N_{PNP}	-0.024	-0.023	0.058	-0.009	-0.006	0.066	-0.029	-0.028	0.047
pyr	0.020	0.016	0.103	0.055	0.052	0.144	0.025	0.019	0.089
N_{am}	0.037	0.005	0.147	0.127	0.072	0.207	0.058	0.015	0.162
H_{am}	0.000	0.000	0.005	0.000	0.000	0.007	0.001	0.000	0.007
C6	0.013	0.027	0.069	0.035	0.072	0.144	0.017	0.037	0.089

Table S15. Ligand and metal charges, see Scheme S2, inferred from the analysis of the Löwdin atomic charges and spins predicted using DFT for the amido complexes using unabridged structural models derived from the experimental X-ray structures.

	Löwdin atomic charges								
Fnct.	**b3lyp**			**bp86**			**tpssh**		
S	**1/2**	**1/2**	**3/2**	**1/2**	**1/2**	**3/2**	**1/2**	**1/2**	**3/2**
Cp.	**4a**	**4b**	**4b**	**4a**	**4b**	**4b**	**4a**	**4b**	**4b**
Co	-0.608	-0.573	-0.421	-0.688	-0.652	-0.519	-0.627	-0.589	-0.437
L_{PNP}	0.844	0.875	0.688	0.841	0.874	0.685	0.840	0.870	0.670
L_{am}	-0.043	-0.301	-0.266	0.028	-0.222	-0.166	-0.013	-0.280	-0.233
P_1	1.010	1.011	0.968	0.986	0.988	0.945	0.996	0.997	0.954
P_2	0.997	1.003	0.969	0.977	0.983	0.949	0.985	0.992	0.957
N_{PNP}	0.206	0.208	0.183	0.235	0.237	0.215	0.213	0.214	0.189
pyr	-0.145	-0.146	-0.179	-0.117	-0.117	-0.143	-0.129	-0.131	-0.170
N_{am}	0.280	0.391	0.387	0.328	0.433	0.436	0.291	0.399	0.400
H_{am}	-0.258	-0.379	-0.377	-0.248	-0.366	-0.364	-0.253	-0.372	-0.370
C6	0.141	-0.011	0.022	0.146	0.009	0.054	0.158	0.005	0.044
Löwdin atomic spins									
Co	0.953	0.976	2.419	0.796	0.826	2.172	0.920	0.946	2.369
L_{PNP}	-0.018	0.090	0.340	0.028	0.020	0.441	-0.009	-0.017	0.346
L_{am}	0.059	0.059	0.241	0.156	0.154	0.388	0.080	0.071	0.286
P_1	-0.020	0.024	0.082	-0.017	-0.019	0.097	-0.020	-0.023	0.087
P_2	-0.018	0.016	0.070	-0.012	-0.012	0.089	-0.019	-0.016	0.075
N_{PNP}	0.000	0.000	0.069	0.015	0.017	0.084	0.003	0.003	0.065
pyr	0.035	0.030	0.110	0.067	0.063	0.151	0.043	0.037	0.102
N_{am}	0.040	0.017	0.134	0.101	0.065	0.191	0.055	0.028	0.153
H_{am}	0.008	0.005	0.026	0.017	0.015	0.038	0.010	0.007	0.030
C6	0.014	0.033	0.076	0.042	0.071	0.149	0.020	0.034	0.097

Table S16. Ligand and metal charges, see Scheme S2, derived from the natural population analysis using DFT predicted SCF density of the amido complexes using unabridged structural models derived from experimental X-ray structures.

Natural atomic charges								
Fnct.	**b3lyp[a]**		**bp86**			**tpssh**		
S	**1/2**	**3/2**	**1/2**	**1/2**	**3/2**	**1/2**	**1/2**	**3/2**
Cp.	**4b**	**4b**	**4a**	**4b**	**4b**	**4a**	**4b**	**4b**
Co	0.570	1.013	0.357	0.352	0.779	0.531	0.520	0.975
L_{PNP}	0.027	-0.402	0.086	0.122	-0.314	0.011	0.046	-0.411
L_{am}	-0.597	-0.610	-1.263	-0.474	-0.464	-1.288	-0.566	-0.564
P_1	1.058	0.874	1.050	1.068	0.882	1.021	1.040	0.849
P_2	0.973	0.837	0.978	0.982	0.845	0.953	0.957	0.814
N_{PNP}	-0.582	-0.682	-0.516	-0.512	-0.607	-0.570	-0.564	-0.667
pyr	-0.949	-1.051	-0.902	-0.907	-0.997	-0.928	-0.933	-1.046
N_{am}	-0.814	-0.861	-0.773	-0.705	-0.744	-0.856	-0.782	-0.820
H_{am}	0.289	0.290	0.319	0.290	0.293	0.315	0.287	0.287
C6	-0.791	-0.759	-1.597	-0.813	-0.768	-1.472	-0.779	-0.741
Natural atomic spins								
Co	0.951	2.270	0.741	0.782	1.993	0.880	0.917	2.217
L_{PNP}	-0.008	0.450	0.050	0.043	0.570	0.013	0.003	0.455
L_{am}	0.057	0.280	0.182	0.175	0.437	0.094	0.080	0.328
P_1	-0.021	0.146	-0.010	-0.016	0.168	-0.010	-0.019	0.154
P_2	-0.011	0.120	-0.010	-0.006	0.148	-0.014	-0.008	0.128
N_{PNP}	0.002	0.109	0.024	0.025	0.134	0.005	0.005	0.106
pyr	0.037	0.144	0.081	0.075	0.196	0.051	0.044	0.137
N_{am}	0.031	0.222	0.164	0.109	0.311	0.090	0.047	0.254
H_{am}	0.001	-0.002	-0.001	0.000	-0.002	0.000	0.000	-0.003
C6	0.025	0.060	0.032	0.068	0.131	0.014	0.033	0.079

a) Natural population analysis failed to complete for **4a**.

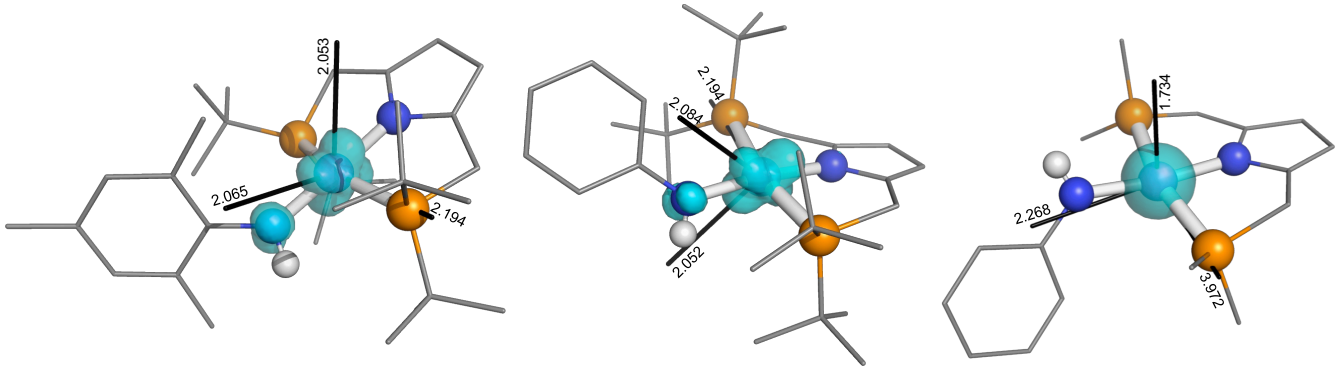

4a
S = 1/2, BP86/def2-TZVPP

4b
S = 1/2, BP86/def2-TZVPP

4b – simplified model
S = 1/2, CAS(7,11)/def2-TZVPP

Figure S13. Plots of the predicted spin densities obtained for **4a** (*left*) and **4b** (*middle*) at the BP86/def2-TZVPP level of theory using unabridged structural models derived from the experimental structures. In addition, shown on the *right* is the CAS(7,11) predicted spin density obtained for a simplified structural model derived from the experimental structure of **4b**. These plots were obtained using an isosurface value of ±0.008. Spin-up, α spin density is shown in purple and spin-down, β spin density is shown in cyan. The axes, shown in black, and their labels indicate the orientation and principal values of the corresponding theoretical **g** tensors. Except for H_{am} all other hydrogen atoms are omitted.

Table S17. DFT-predicted reduced Mulliken orbital charges and spins for the cobalt ion the amido complex using an unabridged structural model derived from the experimental X-ray structure.

	Mulliken reduced orbital charges								
Fnct.	**b3lyp**			**bp86**			**tpssh**		
S	**1/2**	**1/2**	**3/2**	**1/2**	**1/2**	**3/2**	**1/2**	**1/2**	**3/2**
Cmp.	**4a**	**4b**	**4b**	**4a**	**4b**	**4b**	**4a**	**4b**	**4b**
d*z*²	1.882	1.885	1.455	1.876	1.884	1.485	1.870	1.866	1.318
d*xz*	1.171	1.161	1.349	1.297	1.279	1.377	1.217	1.206	1.461
d*yz*	1.892	1.888	1.795	1.844	1.843	1.821	1.881	1.873	1.789
d*x*²-*y*²	0.856	0.901	1.434	0.957	1.005	1.465	0.873	0.900	1.393
d*xy*	1.896	1.893	1.520	1.847	1.835	1.549	1.888	1.887	1.600
Mulliken reduced orbital spins									
d*z*²	0.036	0.045	0.509	0.019	0.021	0.463	0.030	0.044	0.638
d*xz*	0.811	0.829	0.655	0.669	0.697	0.615	0.772	0.790	0.549
d*yz*	0.012	0.014	0.146	0.016	0.017	0.093	0.013	0.017	0.146
d*x*²-*y*²	0.088	0.080	0.635	0.065	0.060	0.570	0.095	0.085	0.630
d*xy*	0.018	0.023	0.430	0.031	0.040	0.370	0.020	0.026	0.346

Table S18. DFT-predicted reduced Löwdin orbital charges and spins obtained for the cobalt ions of the amido complexes using unabridged structural models derived from the experimental X-ray structures.

	Löwdin reduced orbital charges								
Fnct.	**b3lyp**			**bp86**			**tpssh**		
S	**1/2**	**1/2**	**3/2**	**1/2**	**1/2**	**3/2**	**1/2**	**1/2**	**3/2**
Cmp.	**4a**	**4b**	**4b**	**4a**	**4b**	**4b**	**4a**	**4b**	**4b**
d*z*²	1.979	1.963	1.530	1.969	1.962	1.558	1.965	1.950	1.396
d*xz*	1.270	1.241	1.422	1.383	1.348	1.441	1.300	1.273	1.521
d*yz*	1.953	1.945	1.849	1.904	1.897	1.871	1.933	1.924	1.839
d*x*²-*y*²	1.164	1.187	1.736	1.241	1.266	1.742	1.191	1.212	1.728
d*xy*	1.982	1.984	1.610	1.926	1.920	1.632	1.966	1.967	1.677
Löwdin reduced orbital spins									
d*z*²	0.034	0.043	0.509	0.018	0.020	0.462	0.028	0.041	0.638
d*xz*	0.807	0.823	0.654	0.669	0.693	0.615	0.770	0.785	0.548
d*yz*	0.012	0.015	0.148	0.016	0.018	0.095	0.014	0.017	0.148
d*x*²-*y*²	0.073	0.064	0.655	0.054	0.047	0.589	0.078	0.065	0.647
d*xy*	0.020	0.025	0.431	0.034	0.043	0.373	0.023	0.029	0.349

Table S19. DFT-predicted natural atomic orbital occupancies obtained for the cobalt site of the amido complex **4b** obtained for an unabridged structural model derived from the experimental X-ray structure.

Fnct.	**S**	**Sp.**	**d***xy*	**d***xz*	**d***yz*	**d***x*²-*y*²	**d***z*²
b3lyp	**1/2**	α	0.980	0.980	0.986	0.553	0.982
		β	0.961	0.175	0.978	0.475	0.944
		α+β	1.941	1.156	1.964	1.028	1.926
	3/2	α	0.985	0.982	0.991	0.972	0.988
		β	0.558	0.346	0.851	0.426	0.482
		α+β	1.542	1.328	1.841	1.398	1.470
bp86	**1/2**	α	0.968	0.975	0.975	0.600	0.977
		β	0.933	0.310	0.964	0.547	0.962
		α+β	1.902	1.285	1.939	1.147	1.939
	3/2	α	0.977	0.978	0.985	0.957	0.985
		β	0.612	0.388	0.900	0.487	0.527
		α+β	1.590	1.366	1.885	1.444	1.512
tpssh	**1/2**	α	0.976	0.978	0.982	0.571	0.977
		β	0.954	0.215	0.971	0.492	0.940
		α+β	1.930	1.193	1.953	1.063	1.917
	3/2	α	0.981	0.981	0.989	0.967	0.987
		β	0.638	0.453	0.848	0.429	0.349
		α+β	1.619	1.435	1.836	1.396	1.336

Table S20. DFT-predicted natural atomic orbital spins obtained for the cobalt site of the amido complex **4b** using an unabridged structural model derived from the experimental X-ray structure.

Fnct.	S	d*xy*	d*xz*	d*yz*	dx^2-y^2	dz^2
b3lyp	1/2	0.019	0.805	0.008	0.078	0.038
	3/2	0.427	0.637	0.140	0.546	0.506
bp86	1/2	0.035	0.665	0.011	0.054	0.015
	3/2	0.365	0.591	0.086	0.470	0.458
tpssh	1/2	0.022	0.763	0.011	0.079	0.037
	3/2	0.343	0.528	0.141	0.539	0.638

Table S21. Analysis of the time-dependent (TD) DFT calculations performed for **4b** using an unabridged structural model derived from the experimental X-ray structure.

Funct.	TD #	Energy [cm^{-1}]	Initial MO			Final MO			TD coeff.
			MO #	Major Contrib.		MO #	Major Contrib.		
b3lyp	1	3892	140 β	76	z^2	143 β	72	*xz*	0.85
	2	8009	139 β	82	*yz*	143 β	72	*xz*	0.79
	3	9750	137 β	20	*xy*	143 β	72	*xz*	0.16
			135 β	24	*xy*	143 β	72	*xz*	0.11
			138 β	19	*xy*	143 β	72	*xz*	0.15
			142 β	5	*xz*	143 β	72	*xz*	0.33
	4	14746	140 α	76	z^2	144 α	48	x^2-y^2	0.36
			140 β	76	z^2	144 β	37	x^2-y^2	0.34
bp86	1	5009	142 β	77	z^2	143 β	66	*xz*	0.93
	2	8563	140 β	78	*yz*	143 β	66	*xz*	0.94
	3	8983	141 β	36	*xy*	143 β	66	*xz*	0.84
	4	12619	139 β	n.a.	π_{cor}	143 β	66	*xz*	0.99
	5	15352	142 α	81	z^2	144 α	48	x^2-y^2	0.46
			142 β	77	z^2	144 β	49	x^2-y^2	0.51
tpssh	1	5874	140 β	76	z^2	143 β	71	*xz*	0.87
	2	9884	139 β	64	*yz*	143 β	71	*xz*	0.61
			141 β	16	*yz*	143 β	71	*xz*	0.26
	3	10963	138 β	45	*xy*	143 β	71	*xz*	0.24
			142 β	14	*xy*	143 β	71	*xz*	0.59
	4	15942	141 α	65	z^2	144 α	49	x^2-y^2	0.47
			140 β	76	z^2	144 β	47	x^2-y^2	0.39
	5	17092	143 α	6	*xy*	144 α	49	x^2-y^2	0.40
			142 β	14.3	*xy*	144 β	47	x^2-y^2	0.18

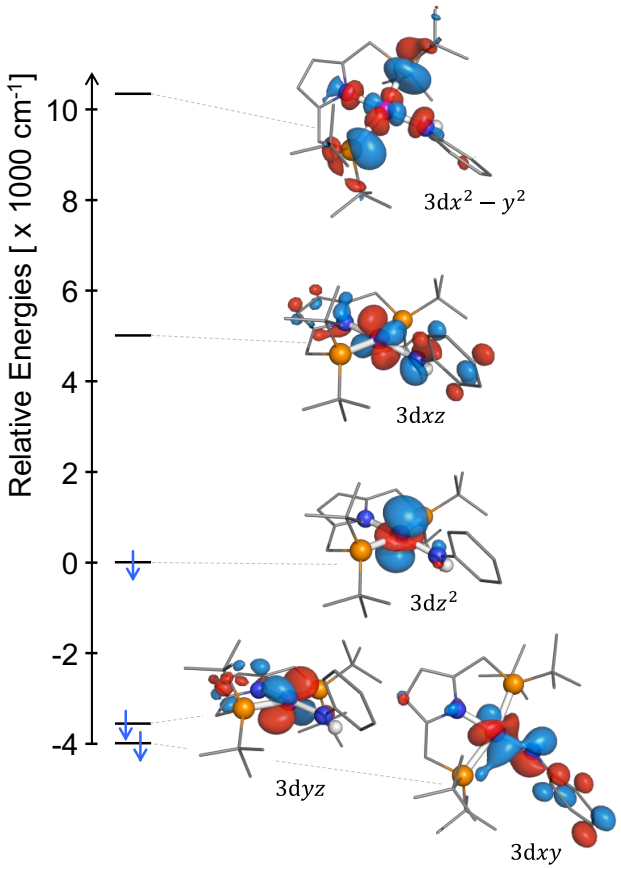

Figure S14. Ligand field splitting diagram inferred for **4b** from the analysis of the one electron excitations predicted by TD DFT at the BP86/def2-TZVPP level of theory. Except for H_{am} all other hydrogen atoms are omitted.

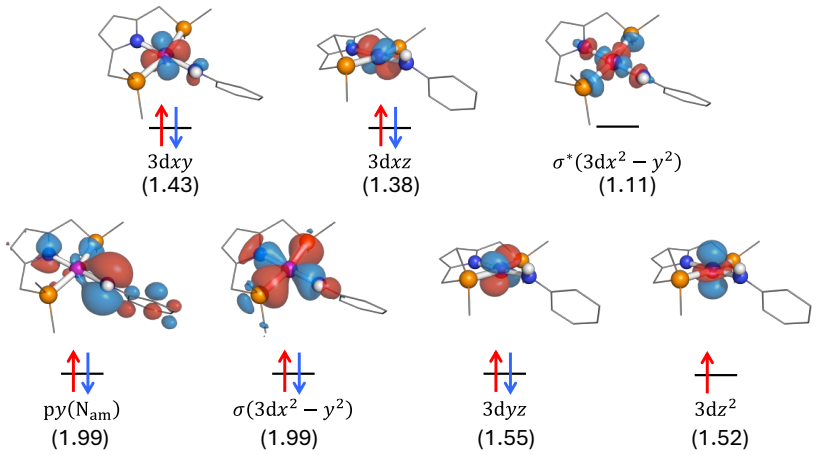

Figure S15. The dominant electronic configuration which contributes 92.5% to the ground state predicted by the CAS(7,11) calculations performed for a simplified structural model of **4b**. These calculations considered 25 doublet, S = 1/2 states. The numbers shown in parentheses indicate the predicted Löwdin orbital populations of the corresponding active space orbitals. Except for H_{am} all other hydrogen atoms are omitted.

Table S22. Theoretical **g** and **A** tensors obtained for the amido complexes.

Method	Cmp.	Principal g values			Principal A values [MHz]			A_{FC} [MHz]	$A_{orbital}$ [MHz]		
b3lyp	**4a**	2.081	2.112	2.323	99	347	418	165	218	66	83
	4b	2.073	2.134	2.365	125	361	463	182	250	89	65
bp86	**4a**	2.054	2.065	2.194	-20	296	323	129	122	41	49
	4b	2.052	2.085	2.222	2	294	371	141	143	61	39
tpssh	**4a**	2.059	2.078	2.183	40	287	359	179	119	49	49
	4b	2.052	2.092	2.203	54	302	416	179	134	61	39
CAS(7,11)	**4b**[a]	1.734	2.268	3.972	not available						
Experimental		*1.853*	*1.994 (2.2)*[b]	*3.288*	*29*	*5 (210)*[b]	*489*	*not available*			

(a) Simplified structural model derived from the experimental structure of **4b**.

(b) Values listed in parentheses were estimated from the peak-to-peak separation of the small ridges found at g ~ 2.2 which appear to originate from a hyperfine splitting not reproduced by our simulations.

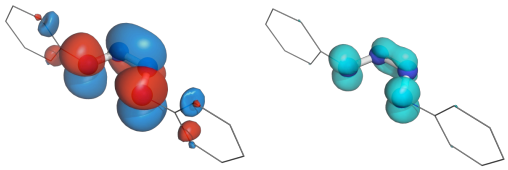

Figure S16. SOMO (*left*) and spin density (right) of the monoanionic tetrazene ligand. When enforcing a C_{2v} point group symmetry for the [N_4] moiety the SOMO has a b_1 symmetry.

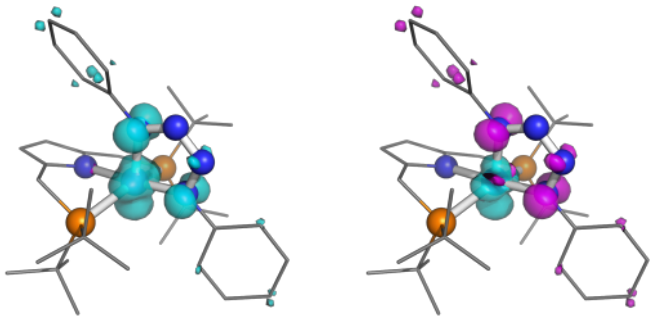

F, S = 1, E = 0 cm^{-1} BS, S = 0, E = 803 cm^{-1}

Figure S17. Spin densities plots obtained for **3** for the F, S = 1 states (*left*) and the BS, S = 0 (*right*) obtained TPSSH/def2-TZVPP (*left*) level of theory. These plots were obtained using an isosurface value of ±0.008. Spin-up, α spin density is shown in purple and spin-down, β spin density is shown in cyan.

Table S23. Ligand and metal charges, see Scheme S2, inferred from the analysis of the Mulliken atomic charges and spins predicted using DFT for the tetrazido complex **3** using an unabridged structural model derived from experimental X-ray structure.

Mulliken atomic charges									
Funct.	**b3lyp**			**bp86**			**tpssh**		
S	**0**	**1**	**2**	**0**	**1**	**2**	**0**	**1**	**2**
Co	0.113	0.128	0.250	-0.100	-0.083	0.014	0.037	0.055	0.174
L_{PNP}	0.140	0.155	0.046	0.287	0.294	0.252	0.164	0.170	0.070
L_{ttrzn}	-0.253	-0.282	-0.296	-0.187	-0.211	-0.266	-0.200	-0.225	-0.244
P_1	0.212	0.213	0.199	0.186	0.192	0.187	0.045	0.046	0.033
P_2	0.154	0.146	0.115	0.133	0.121	0.104	-0.045	-0.054	-0.085
Pyr	-0.722	-0.715	-0.738	-0.723	-0.718	-0.695	-0.629	-0.625	-0.636
N_{PNP}	-0.091	-0.087	-0.139	-0.007	-0.005	-0.038	-0.084	-0.082	-0.134
N_4	-0.292	-0.306	-0.347	-0.165	-0.175	-0.242	-0.238	-0.253	-0.293
Mulliken atomic spins									
Co	-0.833	1.190	2.608	-0.611	1.187	2.455	0.820	1.255	2.610
L_{PNP}	0.099	0.076	0.435	0.053	0.125	0.636	-0.121	0.039	0.426
L_{ttrzn}	0.734	0.734	0.957	0.558	0.688	0.909	-0.699	0.706	0.965
P_1	0.033	0.024	0.108	0.044	0.035	0.143	-0.043	0.010	0.102
P_2	0.051	0.052	0.122	0.021	0.070	0.170	-0.059	0.045	0.118
Pyr	0.006	-0.015	0.167	-0.016	0.004	0.296	-0.010	-0.020	0.192
N_{PNP}	0.016	-0.024	0.094	0.008	-0.020	0.142	-0.021	-0.031	0.096
N_4	0.563	0.548	0.743	0.395	0.481	0.664	-0.529	0.516	0.738

Table S24. Ligand and metal charges, see Scheme S2, inferred from the analysis of the Löwdin atomic charges and spins predicted using DFT for the tetrazido complex **3** using an unabridged structural model derived from experimental X-ray structure.

Löwdin atomic charges									
Funct.	**b3lyp**			**bp86**			**tpssh**		
S	**0**	**1**	**2**	**0**	**1**	**2**	**0**	**1**	**2**
Co	-0.679	-0.661	-0.527	-0.729	-0.712	-0.603	-0.690	-0.675	-0.549
L_{PNP}	0.834	0.852	0.736	0.896	0.906	0.835	0.857	0.868	0.759
L_{ttrzn}	-0.155	-0.191	-0.209	-0.167	-0.194	-0.232	-0.168	-0.193	-0.211
P_1	1.011	1.014	0.984	0.998	1.002	0.972	1.004	1.007	0.977
P_2	1.009	1.008	0.977	1.001	0.998	0.967	1.002	1.001	0.970
Pyr	-0.158	-0.155	-0.163	-0.130	-0.129	-0.087	-0.143	-0.142	-0.140
N_{PNP}	0.225	0.225	0.199	0.250	0.250	0.239	0.232	0.232	0.209
N_4	0.178	0.160	0.136	0.203	0.191	0.157	0.176	0.163	0.141
Löwdin atomic charges									
Co	-0.753	1.182	2.610	-0.512	1.144	2.427	0.687	1.207	2.578
L_{PNP}	0.032	0.095	0.450	-0.037	0.173	0.648	-0.020	0.100	0.485
L_{ttrzn}	0.721	0.723	0.940	0.550	0.683	0.925	-0.667	0.693	0.937
P_1	0.008	0.025	0.084	0.004	0.041	0.105	-0.006	0.026	0.088
P_2	0.023	0.042	0.103	-0.002	0.059	0.128	-0.021	0.043	0.109
Pyr	-0.001	-0.010	0.168	-0.027	0.016	0.286	0.005	-0.009	0.190
N_{PNP}	0.005	-0.014	0.097	-0.010	-0.001	0.142	-0.002	-0.014	0.104
N_4	0.510	0.502	0.688	0.359	0.447	0.642	-0.461	0.469	0.674

Table S25. Ligand and metal charges, see Scheme S2, inferred from the analysis of the natural atomic charges and spins predicted using DFT for the tetrazido complex **3** using an unabridged structural model derived from experimental X-ray structure.

Natural atomic charges									
Funct.	**b3lyp**			**bp86**			**tpssh**		
S	**0**	**1**	**2**	**0**	**1**	**2**	**0**	**1**	**2**
Co	0.753	0.778	1.146	0.592	0.624	0.947	0.722	0.747	1.109
L_{PNP}	-0.043	-0.026	-0.287	0.095	0.097	-0.090	-0.004	0.004	-0.251
L_{ttrzn}	-0.710	-0.753	-0.859	-0.687	-0.721	-0.856	-0.718	-0.751	-0.857
P_1	0.939	0.951	0.865	0.955	0.969	0.883	0.931	0.940	0.849
P_2	0.971	0.964	0.869	1.007	0.988	0.891	0.962	0.954	0.854
Pyr	-0.951	-0.948	-1.012	-0.920	-0.922	-0.905	-0.938	-0.938	-0.987
N_{PNP}	-0.561	-0.561	-0.660	-0.507	-0.510	-0.569	-0.547	-0.548	-0.640
N_4	-0.934	-0.961	-1.074	-0.870	-0.888	-1.022	-0.929	-0.950	-1.062
Natural atomic charges									
Co	-0.733	1.070	2.358	-0.470	1.011	2.129	0.662	1.090	2.313
L_{PNP}	0.027	0.140	0.583	-0.048	0.227	0.810	-0.015	0.147	0.625
L_{ttrzn}	0.707	0.790	1.059	0.519	0.762	1.061	-0.647	0.763	1.062
P_1	0.005	0.052	0.150	0.007	0.075	0.182	-0.004	0.055	0.158
P_2	0.020	0.077	0.163	-0.020	0.103	0.203	-0.018	0.081	0.173
Pyr	0.005	-0.015	0.214	-0.020	0.011	0.352	-0.001	-0.014	0.241
N_{PNP}	0.011	-0.021	0.153	-0.005	-0.006	0.218	-0.008	-0.020	0.164
N_4	0.538	0.623	0.869	0.353	0.572	0.836	-0.479	0.591	0.861

Table S26. DFT-predicted reduced Mulliken orbital charges and spins for the cobalt ion the tetrazido complex **3** using an unabridged structural model derived from the experimental X-ray structure.

Mulliken reduced orbital charges									
Funct.	**b3lyp**			**bp86**			**tpssh**		
S	**0**	**1**	**2**	**0**	**1**	**2**	**0**	**1**	**2**
dz^2	1.024	1.045	1.211	1.151	1.153	1.277	1.057	1.070	1.230
d*xz*	1.973	1.979	1.496	1.953	1.960	1.387	1.986	1.993	1.546
d*yz*	1.839	1.793	1.664	1.755	1.732	1.724	1.808	1.786	1.653
dx^2-y^2	0.910	0.934	1.409	1.054	1.068	1.456	0.940	0.958	1.396
d*xy*	1.891	1.860	1.626	1.836	1.813	1.713	1.890	1.853	1.632
Mulliken reduced orbital spins									
dz^2	-0.693	0.690	0.735	-0.572	0.592	0.656	0.667	0.677	0.717
d*xz*	-0.011	0.010	0.505	-0.019	0.018	0.605	0.014	0.012	0.471
d*yz*	0.090	0.163	0.313	0.157	0.206	0.241	-0.123	0.175	0.333
dx^2-y^2	-0.179	0.188	0.640	-0.140	0.165	0.581	0.180	0.199	0.631
d*xy*	0.050	0.098	0.349	0.076	0.122	0.243	-0.058	0.114	0.352

Table S27. DFT-predicted reduced Löwdin orbital charges and spins for the cobalt ion the tetrazido complex **3** using an unabridged structural model derived from the experimental X-ray structure.

Löwdin reduced orbital charges									
Funct.	**b3lyp**			**bp86**			**tpssh**		
S	**0**	**1**	**2**	**0**	**1**	**2**	**0**	**1**	**2**
dz^2	1.222	1.243	1.409	1.325	1.328	1.449	1.243	1.256	1.418
d*xz*	2.018	2.024	1.553	1.988	1.994	1.438	2.011	2.018	1.582
d*yz*	1.942	1.899	1.772	1.854	1.833	1.825	1.900	1.880	1.748
dx^2-y^2	1.175	1.200	1.696	1.297	1.311	1.717	1.217	1.236	1.702
d*xy*	1.965	1.937	1.705	1.899	1.879	1.780	1.946	1.911	1.693
Löwdin reduced orbital spins									
dz^2	-0.663	0.662	0.713	-0.540	0.562	0.635	0.633	0.645	0.692
d*xz*	-0.011	0.011	0.502	-0.015	0.017	0.602	0.011	0.011	0.467
d*yz*	0.105	0.172	0.327	0.170	0.210	0.249	-0.140	0.182	0.345
dx^2-y^2	-0.160	0.170	0.655	-0.121	0.145	0.596	0.158	0.173	0.641
d*xy*	0.055	0.105	0.357	0.080	0.127	0.251	-0.063	0.121	0.361

Table S28. DFT-predicted natural atomic orbital occupancies obtained for the cobalt site of the tetrazido complex **3** obtained for an unabridged structural model derived from the experimental X-ray structure.

Fnct.	S	Sp.	3d*xy*	3d*xz*	3d*yz*	3dx^2-y^2	3dz^2	total
b3lyp	0	α	0.980	0.973	0.982	0.432	0.218	3.585
		β	0.936	0.981	0.905	0.596	0.888	4.305
		α+β	1.916	1.954	1.887	1.028	1.105	7.890
	1	α	0.984	0.982	0.988	0.614	0.894	4.462
		β	0.901	0.977	0.853	0.440	0.229	3.399
		α+β	1.884	1.959	1.841	1.054	1.124	7.861
	2	α	0.984	0.981	0.987	0.976	0.983	4.910
		β	0.654	0.494	0.703	0.426	0.281	2.558
		α+β	1.637	1.475	1.691	1.402	1.264	7.468
bp86	0	α	0.968	0.963	0.979	0.536	0.346	3.792
		β	0.897	0.974	0.836	0.653	0.890	4.251
		α+β	1.866	1.937	1.815	1.188	1.236	8.043
	1	α	0.975	0.976	0.982	0.672	0.899	4.504
		β	0.867	0.966	0.808	0.529	0.335	3.505
		α+β	1.842	1.942	1.790	1.201	1.235	8.009
	2	α	0.978	0.978	0.985	0.968	0.977	4.886
		β	0.753	0.398	0.779	0.490	0.354	2.774
		α+β	1.731	1.376	1.765	1.458	1.331	7.660
tpssh	0	α	0.924	0.979	0.870	0.621	0.888	4.281
		β	0.976	0.970	0.980	0.460	0.247	3.634
		α+β	1.900	1.949	1.850	1.081	1.135	7.915
	1	α	0.981	0.980	0.986	0.639	0.898	4.483
		β	0.881	0.975	0.840	0.461	0.248	3.406
		α+β	1.862	1.955	1.826	1.100	1.145	7.889
	2	α	0.982	0.979	0.986	0.973	0.981	4.902
		β	0.647	0.528	0.685	0.441	0.299	2.600
		α+β	1.629	1.508	1.671	1.414	1.280	7.502

Table S29. DFT-predicted natural atomic orbital occupancies obtained for the cobalt site of the tetrazido complex **3** obtained for an unabridged structural model derived from the experimental X-ray structure.

Fnct.	S	3d*xy*	3d*xz*	3d*yz*	3dx^2-y^2	3dz^2	total
b3lyp	0	0.044	-0.008	0.077	-0.164	-0.670	-0.721
	1	0.083	0.006	0.134	0.175	0.665	1.062
	2	0.330	0.487	0.284	0.550	0.702	2.352
bp86	0	0.071	-0.012	0.143	-0.117	-0.544	-0.458
	1	0.108	0.010	0.175	0.143	0.564	1.000
	2	0.225	0.580	0.206	0.478	0.624	2.112
tpssh	0	-0.053	0.008	-0.109	0.161	0.640	0.647
	1	0.100	0.005	0.145	0.177	0.650	1.078
	2	0.335	0.451	0.302	0.532	0.682	2.301

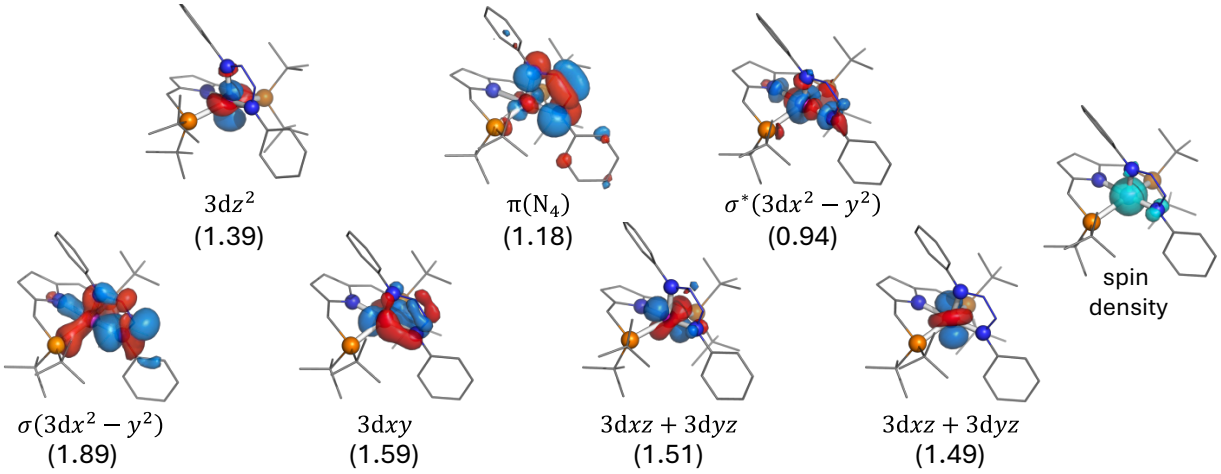

Figure S18. Active space orbitals and predicted spin density (*right*) obtained for the CAS(7,10) calculation of the tetrazene complex **3** which considered 10 S = 1, 25 S = 0 and 10 S = 2 states. The numbers shown in parentheses indicate the predicted Löwdin orbital populations of the corresponding active space orbitals. The major configurations contributing to the ground state are listed in Table S27.

Table 30. The twenty most important contributions to the triplet ground state of **3** predicted by various CAS(7,10) calculations using an unabridged structural model derived from the experimental structure. The orbitals spanning the active space are presented in Figure S18.

#	10 S = 1		10 S = 1, 25 S = 0		10 S = 1, 10 S = 2		10 S = 1, 25 S = 0, 10 S = 2	
	c	*config*	*c*	*config*	*c*	*config*	*c*	*config*
1	0.217	2222101	0.235	2222101	0.160	2122111	0.201	2122111
2	0.170	2222110	0.190	2122111	0.151	2222101	0.198	2222101
3	0.150	2122111	0.142	2222110	0.129	2121211	0.110	2222110
4	0.112	2212201	0.087	2212201	0.104	2221201	0.064	2121211
5	0.088	2112211	0.082	2112211	0.096	2222110	0.057	2221201
6	0.042	2022121	0.038	2022121	0.041	2112211	0.055	2112211
7	0.027	2212210	0.030	2212111	0.040	2022121	0.050	2212111
8	0.025	2121121	0.026	2121121	0.032	2221111	0.040	2022121
9	0.021	2212111	0.022	2221111	0.032	2221210	0.037	2212201
10	0.021	2012221	0.014	2212210	0.031	2212201	0.019	2112121
11	0.014	2221111	0.014	2012221	0.027	2021221	0.013	2221210
12	0.013	2111221	0.012	2211211	0.014	2122120	0.013	2122120
13	0.012	1122121	0.010	2111221	0.014	2212111	0.011	2021221
14	0.009	1222102	0.009	1222102	0.013	2121220	0.010	2221111
15	0.007	2211211	0.008	1122121	0.008	2012221	0.009	2012221
16	0.005	2112220	0.006	2122120	0.007	2122102	0.009	2211211
17	0.005	1022122	0.006	1122112	0.006	2112121	0.007	2122201
18	0.005	1122112	0.005	2211112	0.006	2212210	0.007	1222102
19	0.004	2122120	0.005	2122201	0.006	1122112	0.006	1122112
20	0.004	2211112	0.005	2112121	0.005	2122201	0.006	2212210

Table S31. CAS(7,10) charge and spin distributions predicted for **3**.

Nr St.	10 S = 1		10 S = 1, 25 S = 0		10 S = 1, 10 S = 2		10 S = 1, 25 S = 0, 10 S = 2	
Q/S	**charge**	**spin**	**charge**	**spin**	**charge**	**spin**	**charge**	**spin**
Co	-0.424	2.002	-0.426	0.994	-0.394	2.473	-0.405	1.643
L_{PNP}	0.678	0.043	0.665	0.025	0.629	0.107	0.637	0.073
L_{ttrzn}	-0.254	-0.045	-0.239	-0.018	-0.235	0.420	-0.232	0.283
P_1	1.017	0.010	1.015	0.006	1.008	0.026	1.010	0.018
P_2	1.005	0.009	1.002	0.005	0.995	0.027	0.997	0.018
Pyr	-0.242	0.018	-0.244	0.010	-0.253	0.034	-0.251	0.023
N_{PNP}	0.141	0.012	0.140	0.007	0.133	0.023	0.135	0.016
N_4	0.075	-0.039	0.084	-0.016	0.083	0.338	0.086	0.228

Table S32. Zero field splitting parameters and g tensors derived from the CAS(7,10) calculations of **3**. Values obtained using the effective Hamiltonian approach implemented in ORCA.

CAS(7,10)	D [cm^{-1}]	E/D	principal g-tensor components		
10 S = 1	-87.54	0.122	1.984	2.197	2.979
10 S = 1, 25 S = 00	-165.23	0.037	1.715	2.253	4.802
10 S = 1, 10 S = 2	-179.31	0.025	1.701	2.161	5.118
10 S = 1, 25 S = 0,10 S = 2	-88.54	0.116	1.983	2.203	2.998

S5. Reference

(1) Becke, A. D. Density-Functional Exchange-Energy Approximation with Correct Asymptotic Behavior. *Phys. Rev. A* **1988**, *38* (6), 3098–3100. https://doi.org/10.1103/PhysRevA.38.3098.

(2) Lee, C.; Yang, W.; Parr, R. G. Development of the Colle-Salvetti Correlation-Energy Formula into a Functional of the Electron Density. *Phys. Rev. B* **1988**, *37* (2), 785–789. https://doi.org/10.1103/PhysRevB.37.785.

(3) Perdew, J. P.; Kurth, S.; Zupan, A.; Blaha, P. Accurate Density Functional with Correct Formal Properties: A Step Beyond the Generalized Gradient Approximation. *Phys. Rev. Lett.* **1999**, *82* (12), 2544–2547. https://doi.org/10.1103/PhysRevLett.82.2544.

(4) Barrach, S. M. Population Analysis and Electron Densities from Quantum Mechanics. In *Reviews In computational chemistry*; Reviews In computational chemistry; VCH Publishers, Inc: New York, 1994; Vol. 5, pp 171–227.

(5) Glendening, E. D.; Badenhoop, J. K.; Reed, A. E.; Carpenter, J. E.; Bohmann, J. A.; Morales, C. M.; Karafiloglou, P.; Landis, C. R.; Weinhold, F. NBO 7.0, 2018.

(6) Duboc, C.; Ganyushin, D.; Sivalingam, K.; Collomb, M.-N.; Neese, F. Systematic Theoretical Study of the Zero-Field Splitting in Coordination Complexes of Mn(III). Density Functional Theory versus Multireference Wave Function Approaches. *The Journal of Physical Chemistry A* **2010**, *114* (39), 10750–10758. https://doi.org/10.1021/jp107823s.

(7) Duboc, C. Determination and Prediction of the Magnetic Anisotropy of Mn Ions. *Chemical Society Reviews* **2016**, *45* (21), 5834–5847. https://doi.org/10.1039/C5CS00898K.